5-2005

A Computational Model to Predict In Vivo Lower Limb Kinetics and Assess Total Knee Arthroplasty Design Parameters

Joel Thomas Outten
University of Tennessee - Knoxville

To the Graduate Council:

I am submitting herewith a thesis written by Joel Thomas Outten entitled "A Computational Model to Predict In Vivo Lower Limb Kinetics and Assess Total Knee Arthroplasty Design Parameters." I have examined the final electronic copy of this thesis for form and content and recommend that it be accepted in partial fulfillment of the requirements for the degree of Master of Science, with a major in Engineering Science.

Richard D. Komistek, Major Professor

We have read this thesis and recommend its acceptance:

Mohamed R. Mahfouz, Jack F. Wasserman, Charles H. Aikens

Accepted for the Council:
Dixie L. Thompson

Vice Provost and Dean of the Graduate School

(Original signatures are on file with official student records.)

To the Graduate Council:

I am submitting herewith a thesis written by Joel Thomas Outten entitled "A Computational Model to Predict In Vivo Lower Limb Kinetics and Assess Total Knee Arthroplasty Design Parameters." I have examined the final electronic copy of this thesis for form and content and recommend that it be accepted in partial fulfillment of the requirements for the degree of Master of Science with a major in Engineering Science.

Richard D. Komistek
Major Professor

We have read this thesis
and recommend its acceptance:

Mohamed R. Mahfouz

Jack F. Wasserman

Charles H. Aikens

Accepted for the Council:

Anne Mayhew
Vice Chancellor and Dean of
Graduate Studies

(Original signatures are on file with official student records.)

A Computational Model to Predict In Vivo Lower Limb Kinetics and Assess Total Knee Arthroplasty Design Parameters

A Thesis Presented for the
Master of Science Degree
The University of Tennessee, Knoxville

Joel Thomas Outten
May 2005

Acknowledgements

The author gratefully acknowledges DePuy Orthopaedics, Inc. for funding this study. Also, the author would like to thank the many people who assisted and provided support throughout this study. Specifically, endless thanks to Dan Auger at DePuy, who has constantly provided invaluable guidance and support from the birth of this project. The author greatly appreciates the actual data collection and processing assistance provided by Blair Walden, Raphael McInnis, and Kristen Yoder, as well as the graphics assistance from Gary To and David Holmes. The author feels privileged to have had the opportunity to work with Dr. Thomas Kane, who helped initially guide the construction of the model. Much thanks to Michael Kuhn, who very kindly and selflessly sacrificed his time to add functionalities to the registration software to improve the accuracy of this model. This work would not have been possible without the constant expertise provided by Mathew Anderle and the laboratory management and non-stop troubleshooting of Scott Walker. Thanks to Dr. Mohamed Mahfouz, the driving force and think-tank behind the fluoroscopic registration process, who graciously donated his students' time to assist with this study. Also thanks to him, Dr. Jack Wasserman, and Dr. Hal Aikens for serving on the committee to review this work. Finally, the author feels extremely fortunate to have had the opportunity to conduct this study underneath the guidance of Dr. Richard Komistek. His endless support, encouragement, and insight proved to be invaluable throughout the course of this study. Without his vision, this study would never have come to fruition.

Abstract

Evaluating total knee arthroplasty implant design success generally requires many years of patient follow-up studies which are both inefficient and costly. Although computational modeling is utilized during the implant design phase, it has yet to be fully utilized in order to predict the post-implantation kinetics associated with various design parameters. The objective of this study was to construct a three-dimensional computational model of the human lower limb that could predict *in vivo* kinetics based upon input subject specific kinematics. The model was constructed utilizing Kane's theory of dynamics and applied to two clinical sub-studies. Firstly, axial tibiofemoral forces were compared over a deep knee bend between normal knee subjects and those with implanted knees. Secondly, kinematics were obtained for a sample subject undergoing a deep knee bend, and the amount of femoral rollback experienced by the subject (-1.86 mm) was varied in order to evaluate the subsequent change in the axial tibiofemoral contact force and the quadriceps force. The mean axial tibiofemoral contact force was 1.35xBW and 2.99xBW for the normal and implanted subjects, respectively, which was a significant difference ($p = 0.0023$). The sample subject experienced a decrease in both the axial tibiofemoral contact force (-8.97%) and the quadriceps load (-11.84%) with an increase of femoral rollback to -6 mm. A decrease in rollback to 6 mm led to increases in both the contact force (22.45%) and the quadriceps load (27.14%). These initial studies provide evidence that this model accurately predicts *in vivo* kinetics and that kinetics depend on implant design and patient kinematics.

Table of Contents

List of Tables

List of Figures

Chapter 1: Introduction

Over time, the design of knee replacements has largely been a *post hoc* process, in which empirical data is obtained after total knee arthroplasty (TKA) in order to evaluate design success. Although theoretical approaches are used towards replacement design, the difficulty of modeling the subsequent kinetic effects after TKA inherently places limits on the extent to which pre-TKA conclusions can be drawn. The primary difficulties involved in modeling *in vivo* knee kinematics are twofold: accurate data collection and the statically indeterminate nature of the system.

The main methods of approximating *in vivo* motions of the rigid components of the knee include: skin markers (Soutas-Little et al., 1987; Andriacchi et al., 1998), bone pins (LaFortune et al., 1992; Ramsey et al., 2003), external fixation devices (Marin et al., 1999; Ganjika et al., 2000; Lin et al., 2003), roentgen stereophotogrammetric analysis (RSA) (Fleming et al., 2002; Saari et al., 2003), and video fluoroscopy (Dennis et al., 1998; Fantozzi et al., 2004). Skin markers are non-invasive and involve no radiation exposure, but have been shown to induce measurement errors of up to 18 degrees for internal/external rotation (Murphy, 1990). Another study found that skin markers produced errors of 21% for flexion/extension, 63% for internal/external rotation, and 70% for abduction/adduction during gait (Reinschmidt et al., 1997). Intra-cortical bone pins have been found to yield highly accurate measurements (with errors less than 0.4 mm) (Ramsey et al., 2003), but the insertion process is highly invasive and stressful, limiting the application of this process to small sample sizes. External linkages attached to the limbs offer a non-invasive approach to bone pins, but assume that there is

negligible mobility between the rigid structure and the underlying bone. Rigid attachments have also been used in patellar tracking, but limitations exist upon the activities that can be analyzed. For example, with one attachment design, positions can only be determined from full extension to 20 degrees of flexion (Lin et al., 2003). RSA yields highly accurate results, but it is often non-weight bearing, utilizes static, and can only be performed when specially designed replacements were implanted at the time of TKA. Video fluoroscopy has proved to be a highly accurate and non-invasive procedure that exposes patients to minimal radiation. Our group employs a novel semi-automated algorithm to register three-dimensional (3-D) computer automated design (CAD) models two dimensional (2-D) fluoroscopy images. This procedure yields *in vivo* 3-D kinematics, susceptible to errors of less than 0.5 mm for in-plane translations and less than 0.5^{o} for in-plane rotations (Mahfouz et al., 2003). We believe that this technology offers the most practical and reliable method for determining knee kinematics. For instance, a different approach to obtaining 3-D kinematics from 2-D video fluoroscopy produces errors of 1.2 mm for in-plane translations, 0.8 degrees for in–plane rotations, and 4.0 mm for medial/lateral translation (Kanisawa et al., 2003).

Aside from obtaining rigid body motions in the knee, determining the *in vivo* contact and soft tissue forces has proven to be extremely difficult due to the statically indeterminant nature of the system. The two primary methods for obtaining *in vivo* contact forces are telemetry and mathematical modeling. Telemetry has traditionally been utilized to determine forces acting at the hip (Rydell, 1965; Bergmann et al., 1993), and, more recently, near the knee (Taylor and Walker, 2001), to give very accurate results for axial forces, torques, and bending moments. However, the requisite instrumented

prostheses are very expensive and prevent studies involving more than a few subjects. The more practical alternative is mathematical modeling, which can be applied to an infinite sample size. However, the leg is controlled by 47 muscles (Crowninshield and Brand, 1981), which creates a statically indeterminant system. This dilemma has been handled either by applying optimization criteria (Crowninshield et al., 1975; Seireg and Avrikar, 1975) or by reducing the amount of unknowns involved (Paul, 1965; Komistek et al., 1998; Lloyd and Besier, 2003). Although optimization can yield solutions from indeterminate problems, it has the potential to yield physiologically unrealistic, although mathematically sound, calculations (Challis, 1997). Although the reduction technique can create a statically determinant system, there are often too many degrees of freedom (DOFs), or too many unknowns to create an efficient algorithm. To this end, Kane's theory of multi-body dynamics (Kane and Levinson, 1985), which uses a simultaneous approach to eliminate redundancy within the dynamical equations themselves, can greatly facilitate computational speed and reliability.

The goal of this work was to create a 3-D model of the human knee that would generate accurate *in vivo* contact forces for the lower limb. Specifically, the aim was to model kinetics of the tibiofemoral joint, the patellofemoral joint, the hip joint, and soft tissue forces surrounding the knee. The constructed model utilizes input kinematics from the fluoroscopic registration process, and outputs the associated kinetics. Hence, the model relies on an inverse dynamics approach. Although various optimization criteria could be used to solve the full lower limb indeterminate system, this study was more concerned with the primary kinetics of the lower limb, such as the joint contact forces and extensor mechanism loads. Therefore, the reduction approach (the amount of

unknowns are reduced to a statically solvable system) was chosen to create a solvable system. To maximize computational efficiency, Kane's dynamical equations of motion were used to solve the system.

In addition to the construction of the computational model, this study incorporated two clinical applications of the model. Firstly, it was applied to two sample subject groups, normal knee and TKA subjects, undergoing a deep knee bend (DKB) activity and used to compare the axial tibiofemoral forces between the two groups. Secondly, the model was applied to a sample TKA patient undergoing a DKB. The anterior-posterior (AP) translation of the femorotibial contacts upon the tibial plateau were varied over the activity to simulate both more anterior translation and more posterior translation (or rollback) than the original subject experienced. The axial tibiofemoral contact force and the quadriceps load were determined for each condition, and then compared to evaluate the effect of rollback upon knee kinetics.

This study was part of a larger effort to create a computational model that will assist TKA implant design by simulating the kinetic effects produced by particular design parameters. The focus of the model is to allow for adjustment of constraints and parameters to simulate a given total knee replacement design. The applicability and efficacy of the design will then be evaluated by comparing the TKA results with those of the normal knee, as well as to other designs. This model will thus provide quantitative, theoretical data that will provide guidance and insight towards determining the *in vivo* success of TKA designs prior to implantation and/or manufacture.

Chapter 2: Materials and Methods

This study consisted of two main divisions:

1. Construction of the computational knee model
2. Application of the model to obtain clinically relevant results.

The construction of the model consisted of applying the concepts of Kane's method of dynamics to the human knee. This entailed creation of a lower limb model utilizing Autolev^{TM}, a software package that provides a user-interface that is constructed specifically for dynamics modeling built upon Kane's method. The model was designed to accept kinematics from the 3-D fluoroscopic registration process, both for normal knee subjects and TKA subjects undergoing a DKB. Hence, Chapter 3.1 is separated into 3 main sections: Theory, Model, and Kinematics.

Application of the model was carried out by obtaining kinematics from fluoroscopic data of previously analyzed subjects. The first application consisted of comparing the tibiofemoral contact forces of subjects with normal knees to those of subjects with total knee replacements (TKRs). This application involved obtaining kinematics for seven subjects in each group, running the model for each subject, then tabulated and comparing results between the groups. The second application focused on predicting the *in vivo* kinetics of only one patient, and then varying the anterior-posterior (AP) motion of the femur in order to evaluate the kinetic effects of femoral rollback. These two applications of the computational model will be discussed separately.

2.1: Construction of the Computational Knee Model

2.1.1: Theory

The essential foundation of this study was to construct a rigid body dynamics model of the knee that could be used to predict *in vivo* knee kinetics. This model was proposed to be an inverse dynamics model, implying that kinematics would be input, and kinetics would be output. As with all dynamics models, a system of equations would need to be established and unknowns would then be determined. Due to its computational efficiency, it was decided that Kane's theory of dynamics would allow for the construction of the most ideal model.

Kane's theory of dynamics is founded upon the concept that traditional methods of solving dynamics systems are unnecessarily laborious (Kane and Levinson, 1985). Given a system of multiple rigid bodies, Newtonian and Lagrangian mechanics both solve equations of motion for each rigid body separately. Given a contact between two bodies in a 3-D system, there will be three contact forces exerted by each body upon the other. These forces will each appear twice within the equations of motion in Newtonian and Lagrangian mechanics, once for each body. Kane's method considers all bodies simultaneously and eliminates the redundancy of this process. This can greatly increase computational efficiency for multi-body systems.

Kane's method achieves its efficiency by introducing the abstract concepts of generalized speeds and generalized active forces. Generalized speeds are variables that characterize the speed of a particle, body, or set of particles or bodies in reference to some coordinate system. These can represent either translation velocities or, in the case of bodies, angular velocities. In the simplest case, consider a particle A in reference

frame N. The velocity of A in N, ${}^N v^A$, can be represented by utilizing generalized speeds in the form

$$ {}^N v^A = u_1 N_1 + u_2 N_2 + u_3 N_3, \tag{2.1.1} $$

where u_1, u_2, and u_3 are generalized speeds of A in N. Note that this equation completely characterizes the motion of A in N, and, hence, given the motion of N in another reference frame, will lead to the characterization of the motion of A in that reference frame as well. Similarly, given a body B, its motion in N can be completely characterized utilizing 6 generalized speeds. Defining BO as the mass center of body B and noting that u_1, u_2, and u_3 are defined differently from above, the motion of B is represented by

$$ {}^N v^{BO} = u_1 N_1 + u_2 N_2 + u_3 N_3 \tag{2.1.2} $$

and

$$ {}^N \omega^B = u_4 N_1 + u_5 N_2 + u_6 N_3 \tag{2.1.3} $$

where u_1, u_2, and u_3 characterize the velocity of BO in N and u_4, u_5, and u_6 characterize the angular velocities of B in N. Specifically, these generalized speeds are defined as

$$ u_1 \equiv {}^N v^{BO} \cdot N_1, \qquad u_2 \equiv {}^N v^{BO} \cdot N_2, \qquad u_3 \equiv {}^N v^{BO} \cdot N_3, \tag{2.1.4} $$

$$ u_4 \equiv {}^N \omega^B \cdot N_1, \qquad u_5 \equiv {}^N \omega^B \cdot N_2, \qquad u_6 \equiv {}^N \omega^B \cdot N_3, \tag{2.1.5} $$

where ${}^N \omega^B$ represents the angular velocity of body B in N, and the symbol "·" denotes the dot product.

Although these generalized speeds appear synonymous with the components of the velocity vectors in N, they are handled completely differently. They are incorporated into the angular and translational velocity vectors through the use of partial angular

velocities and partial velocities. Using the same variables as above for body B in N and for *n* generalized speeds, the angular velocity and velocity vectors are written as

$$ {}^{N}v^{BO} = \sum_{r=1}^{n} {}^{N}\tilde{v}_r^{BO} u_r + \tilde{v}_0 \tag{2.1.6} $$

and

$$ {}^{N}\omega^{B} = \sum_{r=1}^{n} {}^{N}\tilde{\omega}_r^{B} u_r + \tilde{\omega}_0 \tag{2.1.7} $$

where ${}^{N}\tilde{v}_r^{BO}$ is called the r[th] (constrained) partial velocity of BO in N, $\tilde{v}_0$ is the (constrained) velocity remainder of BO in A, ${}^{N}\tilde{\omega}_r^{B}$ is the r[th] (constrained) partial angular velocity of B in N, and $\tilde{\omega}_0$ is the (constrained) angular velocity remainder of B in N. Generally, *n* may be greater than the number of degrees of freedom within a system, implying that at least two of the generalized speeds are not independent of each other. In this situation, the previously defined terms are deemed *unconstrained*. When n is equal to the number of degrees of freedom in a system, than the terms are *constrained*. The system utilized in this study was constrained. Therefore, for efficiency and simplicity, all derived terms will be constrained, and the unconstrained system will not be considered. By equating equation (2.1.2) to (2.1.6) and (2.1.3) to (2.1.7), it follows that

$$ {}^{N}\tilde{v}_1^{BO} = N_1, \qquad {}^{N}\tilde{v}_2^{BO} = N_2, \qquad {}^{N}\tilde{v}_3^{BO} = N_3, \qquad \tilde{v}_0 = 0, \tag{2.1.8} $$

$$ {}^{N}\tilde{\omega}_1^{B_0} = N_1, \qquad {}^{N}\tilde{\omega}_2^{B_0} = N_2, \qquad {}^{N}\tilde{\omega}_3^{B_0} = N_3, \qquad \tilde{\omega}_0 = 0. \tag{2.1.9} $$

Hence, if there is no generalized speed associated with a particular unit vector of a reference frame, then that unit vector will not appear within the partial velocity terms.

Now, denote a set S of *v* particles, at which forces (both contact and distance) are acting, as P_i (i =1…*v*). For each generalized speed there is a corresponding force term called a (constrained) generalized active force for S in N. The (constrained) generalized active forces are defined by

$$\tilde{F}_r \equiv \sum_{i=1}^{v} {}^N\tilde{v}_r^{P_i} \cdot R_i \qquad (r = 1,\ldots,n), \tag{2.1.10}$$

where ${}^N\tilde{v}_r^{P_i}$ are the (constrained) partial velocities of P_i (i =1…*v*) and R_i is the resultant of all contact forces and distance forces acting on P_i (i =1…*v*). This equation implies several details fundamental to Kane's method. Firstly, if a certain particle of S does not have a partial velocity associated with it, then forces acting upon this particle will not be included within the generalized active force term. From equations (2.1.2), (2.1.4), and (2.1.6), in order for a point to have a partial velocity associated with it, its velocity must be given in terms of at least one generalized speed. Otherwise, the forces at this particle will be non-contributing forces, and will not be contained in the eventual dynamical equations. Secondly, only the resultant, R_i, of forces upon P_i is considered. Therefore, couple resultants will not be present within the generalized active force equation, and will not be contained within the eventual dynamical equations.

Equation (2.1.10) pertained to a set of particles, but the focus of this study was upon rigid bodies. Equation (2.1.10) can also be applied to points of rigid bodies, but torques must be taken into account as well. Any set of forces acting upon a rigid body can be replaced with a resultant vector, say R, and a couple of torque T. Let Q be the point of B through which R acts. The contribution of this set of forces to the (constrained) generalized active force equation is

$$(\tilde{F}_r)_B = {}^N\tilde{\omega}_r^B \cdot T + {}^N\tilde{v}_r^Q \cdot R \qquad \text{(r = 1,…,n)} \qquad (2.1.11)$$

Similar to equation (2.1.10), this equation implies that in order for forces and torques to appear within the generalized active force equations, the points at which forces act must have velocities written in terms of generalized speeds. Additionally, the angular velocity of the body must be written in terms of generalized speeds in order for torques to be contained within the active force equations.

In addition to active forces acting upon rigid bodies, passive (or inertia) forces must be taken into account when representing the dynamics of the system. For the previously used rigid body B in N, this is done first by determining the inertial force, F^*, and torque, T^*, given by

$$R^* \equiv -M\,{}^N a^{BO} \qquad (2.1.12)$$

and

$$T^* \equiv -\alpha \cdot \underline{I} - \omega \times \underline{I} \cdot \omega, \qquad (2.1.13)$$

where M is the mass of B, ${}^N a^{BO}$ is the acceleration of BO in N, α is the angular acceleration of B in N, ω is the angular velocity of B in N, and $\underline{I}$ is the central inertia dyadic of B. As with the active forces, these terms are incorporated into (constrained) generalized inertia forces for B:

$$(\tilde{F}_r^*)_B = {}^N\tilde{\omega}_r^B \cdot T^* + {}^N\tilde{v}_r^{BO} \cdot R^* \qquad \text{(r = 1,…,n).} \qquad (2.1.14)$$

Once the generalized active and inertia forces are determined, the r dynamical equations, where r is the number of generalized speeds, can be written in order to solve the system:

$$\tilde{F}_r + \tilde{F}_r^* = 0 \qquad \text{(r = 1,…,n).} \qquad (2.1.15)$$

In this study, as previously stated, the number of generalized speeds, *n*, equaled the number of degrees of freedom within the system. Hence, equation (2.1.15) simplifies to

$$F_r + F_r^* = 0 \qquad (r = 1,\ldots,n) \qquad (2.1.16)$$

which is d'Alembert's Principle. This states that sum of the active forces and the passive forces within a system is equal to zero.

It should be noted that the number of dynamical equations corresponds to the number of generalized speeds utilized within the system. Each dynamical equation corresponds to a specific generalized speed. Any multi-body system contains an infinite number of forces (e.g. the force required to hold two adjacent particles together within a rigid body), but the majority of these forces are non-contributing, and will not appear within the generalized active force equations. Thus, they will not appear within the dynamical equations, and cannot be directly calculated. If a non-contributing force is sought, them auxiliary generalized speeds can be introduced to the system. These are speeds that are equal to zero in reality, but are introduced as variables in order to have the corresponding particles (or bodies, for angular velocities) have corresponding partial velocities. This will subsequently result in the force appearing within the dynamical equations. For inverse dynamics problems, all forces and torques to be determined will be non-contributing. Hence, it is necessary to introduce an auxiliary generalized speed for each unknown that is to be calculated.

2.1.2: Model

An inverse dynamics model of the lower limb was created within the Autolev^{TM} environment based upon the concepts of Kane's method of dynamics presented within the previous section. Simplifying reduction assumptions were made according to which forces would be primarily involved in a DKB. The model contained two rigid bodies representing the femur and tibia (Figures 2.1 and 2.2). Since the system was unconstrained, there were 12 degrees of freedom (6 for each body), and hence, 12 unknowns could be found. The complex hip reactions were replaced with a resultant force, F_H, and a torque, T_H, each with three scalar components. Hence, 6 unknowns were required to model the hip reaction. The tibiofemoral joint was replaced with a resultant force, F_{TF}, and a torque, T_{TF}. F_{TF} was composed of three scalar components, but the component of T_{TF} in the direction of the medial-lateral (ML) axis (flexion-extension torque) was assumed to be zero. This was because it was assumed that the extensor mechanism is the primary activator during a DKB, and no additional torque was needed. Thus, five unknowns were required for the tibiofemoral joint interaction. The patellar ligament force, F_{PL}, was the final unknown quantity. The model was created so that it could be applied to both normal knee subjects and TKA subjects.

Activity

The model was constructed to predict *in vivo* lower limb kinetics throughout weight-bearing flexion. Since gait, which is potentially more clinically applicable than weight-bearing flexion, involves the activation of muscles, such as the soleus and gastrocnemius, outside of the extensor mechanism (Otter et al., 2004), it was decided that

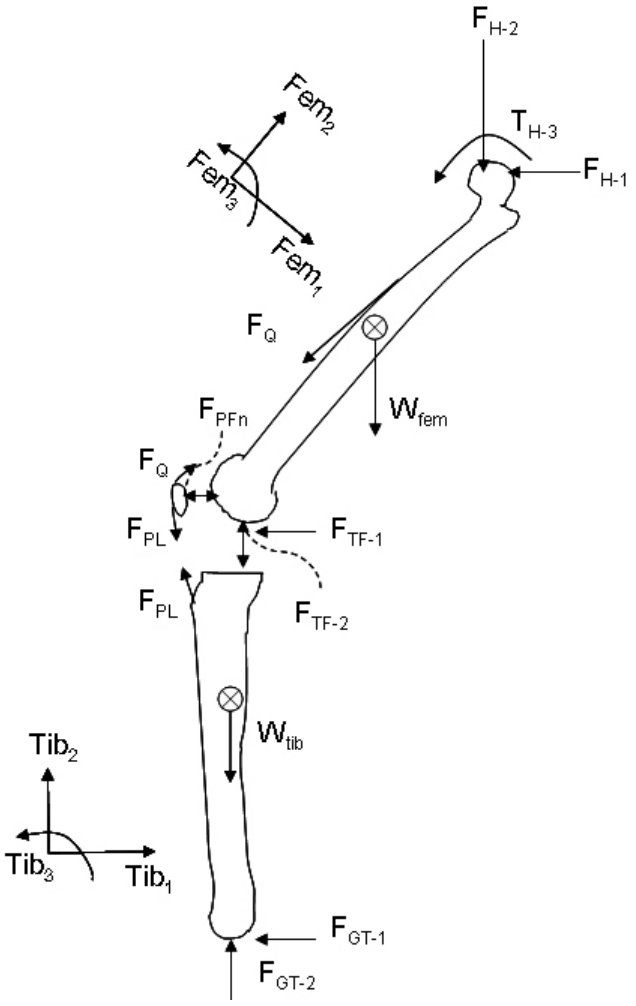

Figure 2.1: Lateral view of free body diagram of lower limb model.

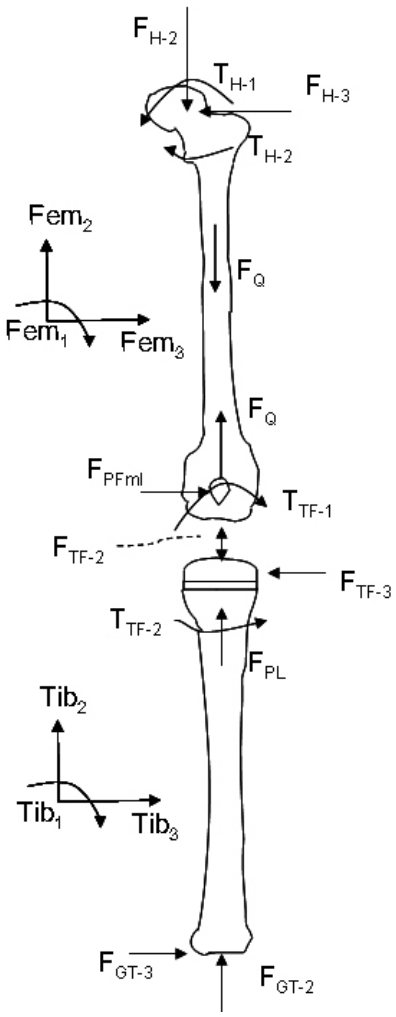

Figure 2.2: Frontal view of free body diagram of lower limb model.

this model would not accurately predict gait kinetics. A deep knee bend (DKB) was the only activity to which the model was applied.

Rigid Body Rotations

The angle of flexion, θ_{flex}, was established as a function of time, t. The DKB activity was assumed, for standardization, to occur from t = 0 to t = 1. Since the initial applications of this model were aimed at assessing varying kinetics due to differences in kinematic patterns over flexion, not specifically the speed of performing the activity, the same temporal function was used for all patients:

$$\theta_{flex} = \frac{\beta_{\max}}{2}\frac{\pi}{180} * \left(1 - \cos\left(\pi * t\right)\right), \tag{2.2.1}$$

where β_{max} represents the maximum flexion angle achieved for the DKB. Figure 2.3 displays θ_{flex} over time for a sample subject that achieved 100º at maximum flexion. This function was chosen because it allows for a gradual increase in flexion at the beginning of the interval, and a gradual decrease at the end of the interval. This was more representative of realistic motions, as opposed to either a linear function or one that

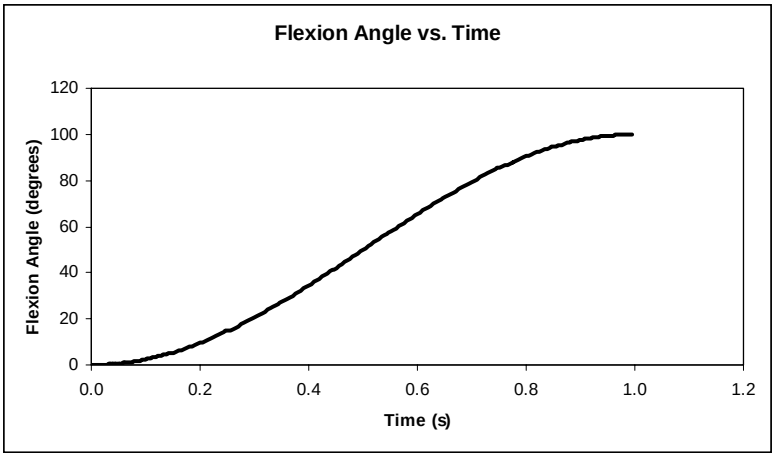

Figure 2.3: Flexion angle versus time for a sample subject with 100º maximum flexion

corresponded to a sudden start (or stop) at the beginning (or end) of the interval.

The orientation and motion of each body was characterized by specifying both the location of a point on each body and the rotations of each body's local reference frame. Specifically, the model was constructed to allow the position of the tibia with respect to the global reference system, N, to be defined in terms of three sequential fixed axis rotations, namely a N_1-N_2-N_3 rotation sequence. These rotations are represented by the variables θ_{Tib-1}, θ_{Tib-2}, and θ_{Tib-3}. The model was constructed to utilize a differentiable polynomial function, in terms of flexion angle, θ_{flex}, to define each rotation over the course of the activity. The order of each equation was adjusted to achieve a high r^2 value. Representing the coefficients of the flexion terms by $c_{1,i},\ldots,c_{n,i}$ for a n^{th} order equation for θ_{Tib-i}, the general function was

$$\theta_{Tib-i} = c_{n,i}\theta_{flex}^{n} + c_{n-1,i}\theta_{flex}^{n-1} + \cdots + c_{1,i}\theta_{flex} + c_{0,i}, \qquad (2.2.2)$$

where $c_{0,i}$ represents the value of θ_{Tib-I} at full extension. The rotations of the femur were specified relative to the tibia by using a 3-2-1 Euler angle sequence in which θ_{flex}, defined by equation (2.2.1), represented the rotation about the Tib_3 axis. Similar to the tibial rotations characterized by equation (2.2.2), the remaining two angles, θ_{fem-1}, θ_{fem-2}, were also defined with differentiable polynomials. Once the rotations of the two bodies were defined, the angular velocity of the tibia in N, ${}^{N}\omega^{Tib}$, and the femur in N, ${}^{N}\omega^{Fem}$, were determined from the cosine matrices. Specifically, these terms were given by

$${}^{N}\omega^{Tib} = \left({}^{N}\frac{dTib_2}{dt} \cdot Tib_3 \right) Tib_1 + \left({}^{N}\frac{dTib_3}{dt} \cdot Tib_1 \right) Tib_2 + \left({}^{N}\frac{dTib_1}{dt} \cdot Tib_2 \right) Tib_3 \qquad (2.2.3)$$

and

$$ {}^{N}\omega^{Fem} = \left({}^{N}\frac{dFem_2}{dt} \cdot Fem_3 \right) Fem_1 + \left({}^{N}\frac{dFem_3}{dt} \cdot Fem_1 \right) Fem_2 $$

$$ + \left({}^{N}\frac{dFem_1}{dt} \cdot Fem_2 \right) Fem_3 , \qquad (2.2.4) $$

where the ${}^{N}\frac{dBody_i}{dt} \cdot Body_j$ terms are found by differentiating the ij[th] element of that body's direction cosine matrix.

The translation of the femur with respect to the tibia was characterized by defining the position vector from a point fixed on the tibia to a point fixed on the femur. The scalar components, in the tibial reference frame, of this vector were defined by polynomial functions dependent upon θ_{flex}.

Morphological Parameters

Population estimates for soft tissue attachment sites and for force application sites were adopted from the literature (White et al., 1989) and are given in Appendices A and C (Tables A.1, A.2, C.1, and C.2). Soft tissue forces, aside from the quadriceps force, were applied in the direction of the positional vector connecting the attachment sites of the proximal and distal ends. The direction of the quadriceps force was applied by assuming an angle to the femoral axis. Since soft tissue weight and geometry, in addition to bone weight and geometry, had to be considered in order to predict realistic kinetics, thigh and shank masses, taken from literature (Pierrynowski and Morrison, 1985) were included within the model (Table A.3, Appendix A). The mass centers for the thigh and shank were determined from a study of 13 cadavers (Hinrichs, 1990), and are given in

Appendix A (Table A.4). The inertial properties of the thigh and shank were calculated using truncated cone, or frustum, theory (Appendix B; Hanavan, 1964) and by obtaining sample measurements of the leg of an average size person (Table B.1). A general body weight of 757 N was assumed for the model, which was the approximate body weight of the sample 24 year old, 1.87 m tall male.

Parameters were entered into the model through the input (.in) file. Autolev^{TM} produced the blank input file, and the morphological parameters were manually entered into the file. A variable parameter was added to the model in order to allow rotation of the entire model around the N_3 axis due to rotation of the original fluoroscopic video, which is frequently encountered.

Ground Reaction Force

In order to take into account body weight, the model was constructed to utilize an input ground-reaction force at the distal end of the tibia. It was assumed that force-plate data would not be readily available for all subjects to which this model would be applied. Therefore, a sample force-plate reaction was taken of the previously mentioned male whose body weight was used for the model. Triaxial force data was taken over the course of a deep knee bend of the right leg (Figure 2.4). The subsequent polynomial equations used to approximate these forces were

$$F_{GT-1} = -6573.7t^6 + 18545t^5 - 19198t^4 + 8940.2t^3 - 1845.7t^2 + 157.32t + 5.1099, \quad (2.2.5)$$

$$F_{GT-2} = -39628t^6 + 130236t^5 - 163569t^4 + 96422t^3 - 25416t^2 + 2090.2t + 344.25, \quad (2.2.6)$$

and

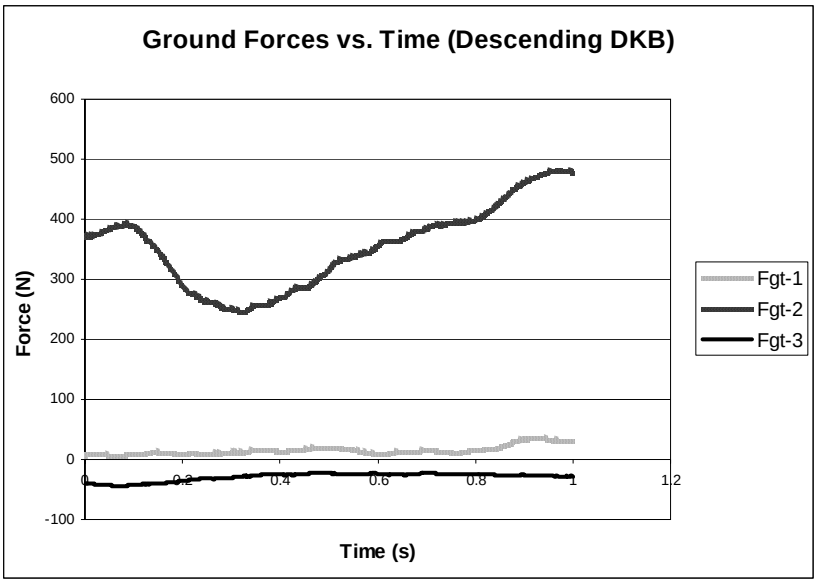

Figure 2.4: Force-plate data for ground reaction force over course of a right leg DKB. Positive F_{GT-1} acts in a posterior direction. Positive F_{GT-2} acts in a superior direction. Positive F_{GT-3} acts in a lateral direction.

$$F_{GT-3} = 1256t^6 - 4539.1t^5 + 6433.7t^4 - 4443.1t^3 + 1443.6t^2 - 140.13t - 39.167, \quad (2.2.7)$$

where each equation produces forces in Newtons. A positive F_{GT-1} value indicates a posteriorly directed force upon the distal end of the tibia, a positive F_{GT-2} value indicates a superiorly directed force, and a positive F_{GT-3} value indicates a laterally directed force. Since this data was taken for a right leg, the application of the computational model to a left leg included reversing the direction of F_{GT-3}.

Patellofemoral Joint

The patellofemoral joint force was assumed to be adequately represented by a normally directed force (normal to the patellar tilt), F_{PFn}, and a ML force, F_{PFml}. Only two components were assumed because, due to articular cartilage, the contact was assumed to be frictionless, and thus the superior-inferior (SI) force was assumed to be 0. The ML force was retained due to the fact that the patella slides within the trochlear

groove during normal motion, particularly during higher degrees of flexion (Hungerford, 1979). It was expected that the sides of the groove would apply a force to the patella in order to resist subluxation. A sagittal view of the patellofemoral joint mechanism is displayed in Figure 2.5, and the subsequent free body diagram is given in Figure 2.6. Assuming that the patellar ligament force, F_{PL}, is known, the remaining forces within the system can be determined. Specifically, the Pat_2 components of the quadriceps force and patellar ligament force must sum to zero. Hence,

$$F_Q(Pat_2 \cdot Q_2) = -F_{PL}(Pat_2 \cdot PL_2). \tag{2.2.8}$$

After calculating the patellar ligament force, the normal component of the patellofemoral force can be similarly determined:

$$F_{PFn} = F_{PL}(Pat_1 \cdot (-PL_2)) + F_Q(Pat_1 \cdot Q_2). \tag{2.2.9}$$

This solves the patellofemoral system in the sagittal plane, but the ML component of the patellofemoral force remains unknown. Figure 2.7 displays a transverse view, from a superior vantage point, of the patellofemoral joint. Although not displayed in the figure, the ML component of the patellar ligament was assumed to be zero. Hence, the ML patellofemoral force can be solved in terms of the quadriceps force:

$$F_{PFml} = -F_Q(Pat_3 \cdot Q_2). \tag{2.2.10}$$

The patellar ligament was assumed to be inextensible, as has been frequently assumed (Shelburne and Pandy, 1997), and the length was taken as 6.45 cm (Clément et al., 1989). This ligament was assumed to remain in the same sagittal plane as the tibia. The patella was assumed to be 5 cm in length from base to apex, and the two patellofemoral forces (F_{PFn} and F_{PFml}) were assumed to be applied at the midpoint of this length. The position

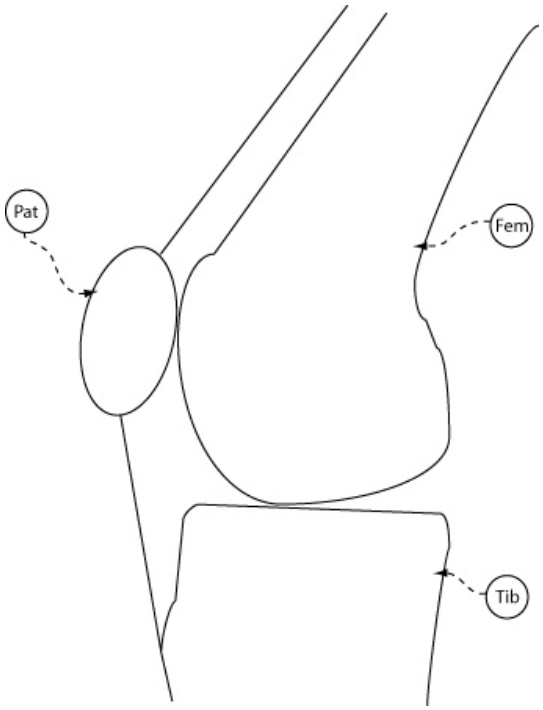

Figure 2.5: Sagittal view of patellofemoral mechanism.

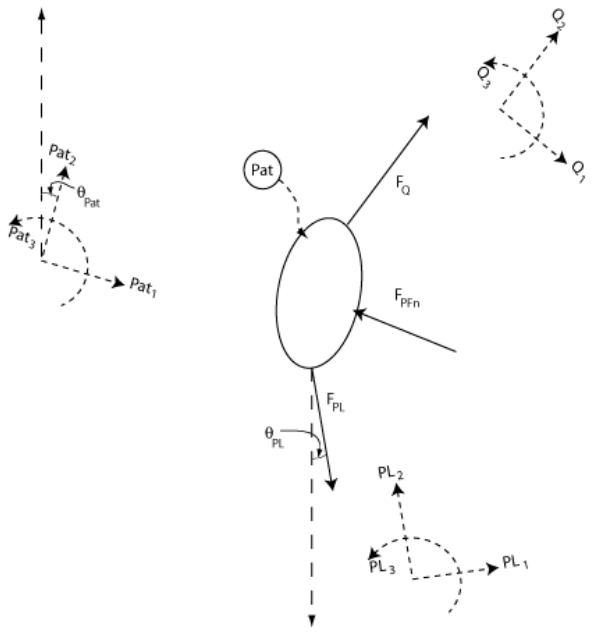

Figure 2.6: Sagittal free body diagram of patella.

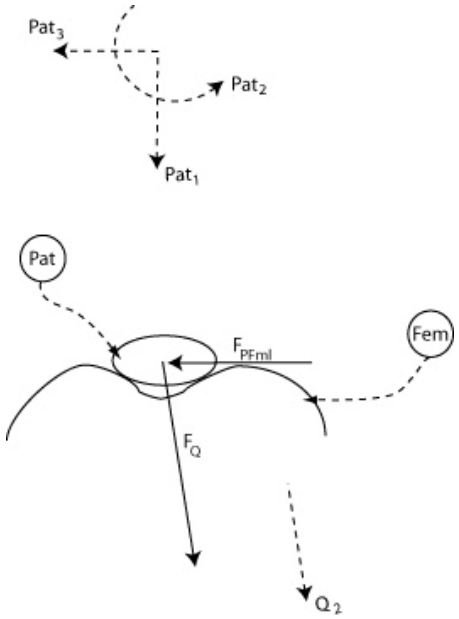

Figure 2.7: Superior view of patello-femoral free body diagram in transverse plane. F_Q acts in the Q_2 direction.

of the patella was characterized by the patellar ligament angle, θ_{PL}, and the patellar tilt angle, θ_{Pat} (Figure 2.6), which were defined as polynomial functions similar to equation (2.2.2). The position of the apex of the patella was characterized by the known length of the patellar ligament and θ_{PL}. θ_{Pat} then allowed for the position of the patella to be completely characterized. As with the patellar ligament, the patella was assumed to reside in the same sagittal plane as the tibia. The quadriceps force was assumed to act within the same sagittal plane as the femur. Since the angle between the quadriceps and the long axis of the femur decreases over flexion (due to the motion of the patella), it was defined by the approximating function

$$\theta_Q = \frac{\pi}{180}(3 - 2.5 * t), \tag{2.2.11}$$

implying that this angle was 3º at full extension and decreased linearly over time to 0.5º at maximum flexion. Since the length of the patella was approximated, the quadriceps force could have been applied in the direction from its origin to the patellar base. However, this model did not account for wrap-around of the quadriceps about the distal anterior femur. Simply utilizing a position vector from the quadriceps origin to the patellar base would have resulted in a negative quadriceps angle, creating a biomechanically unrealistic situation in which contraction of the extensor mechanism aids flexion, rather than resisting it.

Ligaments

The four major ligaments (neglecting the patellar ligament, which has already been discussed) of the knee were incorporated into this model: the lateral collateral

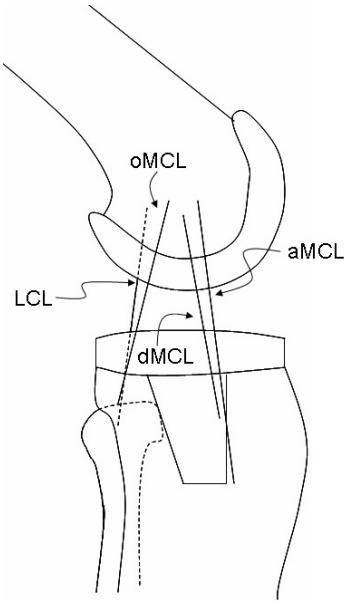

Figure 2.8: Diagram of collateral ligaments in the model, including anterior, oblique, and deep bundles of the MCL.

ligament (LCL), the medial collateral ligament (MCL), the anterior cruciate ligament (ACL), and the posterior cruciate ligament (PCL). The MCL was divided into three bundles (Abdel-Rahman and Hefzy, 1998; Caruntu and Hefzy, 2004): the anterior bundle (aMCL), the oblique bundle (oMCL), and the deep bundle (dMCL), as is shown in Figure 2.8. The LCL was modeled as a single bundle. The ACL was comprised of an anteromedial bundle (aACL) and a posterolateral bundle (pACL) (Arnoczky, 1983; Norwood and Cross, 1979). Similarly, the PCL was divided into a posteromedial bundle (pPCL) and an anterolateral bundle (APCL) (Hughston, 1980; Burks, 1990; Amis, 2003). All ligament attachment sites were adopted from the literature (White et al., 1989; Abdel-Rahman and Hefzy, 1998), and are given in Appendix C (Tables C.1 and C.2). The force-strain equations were assumed to be nonlinear elastic equations given by (Grood and Hefzy, 1982):

$$F_i = k_i \varepsilon_i^2, \qquad \varepsilon_i > 0,$$

$$F_i = 0, \qquad \varepsilon_i \leq 0, \tag{2.2.12}$$

where F_i is the force in ligament *i*, k_i is a stiffness parameter, and ε_i is the ligament strain, given by:

$$\varepsilon_i = \frac{(L_i - L_{0_i})}{L_{0_i}}, \tag{2.2.13}$$

where L_i is the length of ligament *i* and L_{0_i} is the reference length. Autolev^{TM} does not allow piecewise functions, such as equation (2.2.12), to be defined. Therefore, it was necessary to add these equations to the C code directly. All ligament stiffness values (Li et al., 1999b) and reference lengths (Abdel-Rahman and Hefzy, 1998) were determined from previous mathematical models, and are given in Table C.3 (Appendix C).

Autolev^{TM} and C Coding

This model was created within Autolev^{TM}, which then generated a C code for performing the actual calculations and generating results. Four basic codes were generated, according to whether the knee was a right knee facing right or left, or a left knee facing right or left. This was to accommodate the four different variations of subject orientation that occur in fluoroscopic analyses of DKBs. Many variables required knee and direction specific signs (for instance, $+N_3$ is medial for a right knee facing left but lateral for a left knee facing left), so this had to be accounted for in the model. In the interest of brevity and efficiency, only the creation and application of generalized speeds will be discussed. The remaining aspects of the code can be discerned from the

previously discussed features of the model, from the theory of Kane's method, and from the Autolev^{TM} manual (Kane and Levinson, 2000).

After defining the 3-D orientations and motions for the femur and the tibia, auxiliary generalized speeds were introduced. As discussed within Chapter 2.1.1, an auxiliary generalized speed had to be created for each unknown variable to be determined by the model. Specifically, three generalized speeds were created for the angular velocity terms for each body:

$$^{N}\omega^{Tib} = {}^{N}\omega^{Tib} + U_1 * N_1 + U_2 * N_2 + U_3 * N_3, \quad (2.2.14)$$

$$^{N}\omega^{Fem} = {}^{N}\omega^{Fem} + U_4 * N_1 + U_5 * N_2 + U_6 * N_3, \quad (2.2.15)$$

where U_1-U_6 are auxiliary generalized speeds. The remaining 6 auxiliary generalized speeds were introduced at the tibia-ground and tibia-femur interactions as follows:

$$^{N}v^{TG} = U_7 * N_1 + U_8 * N_2 + U_9 * N_3, \quad (2.2.16)$$

$$^{N}v^{FT} = {}^{N}v^{TF} + U_{10} * N_1 + U_{11} * N_2 + U_{12} * N_3, \quad (2.2.17)$$

where $^{N}v^{TG}$ is the velocity of the tibia-ground contact, TG, in N, $^{N}v^{FT}$ is the velocity of the femorotibial contact in N, $^{N}v^{TF}$ is the velocity of the tibiofemoral contact in N, and U_7-U_{12} are auxiliary generalized speeds. In realistic motion, all generalized speeds are equal to zero, but they are needed within the analysis in order to bring the desired unknowns into the generalized active force equations. The 12 subsequent dynamical equations were then utilized to simultaneously solve for the 12 unknowns.

The Autolev^{TM} model generated a 11264 line C code, which was too large to include within this manuscript. The only modifications made directly to the C code were

for the ligament forces given in equation (2.2.12). The force-strain equations were initially defined in Autolev^{TM} as

```
f_mcla=kmcla*strain_mcla^2,                    (2.2.18)
```

which corresponds to the positive strain piecewise segment of equation (2.2.12). This produced the following definition within the C code:

```
F_MCLA = KMCLA*pow(STRAIN_MCLA,2);.            (2.2.19)
```

This definition was replaced with the following coding

```
    if (STRAIN_MCLA < 0)
{
    F_MCLA = 0;
}
    else
{
     F_MCLA = KMCLA*pow(STRAIN_MCLA,2);        (2.2.20)
}
```

which allowed the ligament force-strain relationships to be defined piecewise.

2.1.3: Kinematics Acquisition

Although kinematics could theoretically be obtained from many methods (gait analysis, theoretical equations, etc.) and entered into the model, this model utilized fluoroscopically obtained kinematics. The model was designed to utilize input 3-D kinematics, obtained from a highly accurate 3-D to 2-D registration process (Mahfouz, 2003), as displayed in Figure 2.9. This process utilizes 3-D computer aided design (CAD) models, which are registered to 2-D fluoroscopic images taken from videos of subjects performing activities. For knee implants, these models are constructed based upon the manufacturing specifications. For normal knees, 3-D models are constructed from segmentation of subject specific computed tomography (CT) data (Komistek et al.,

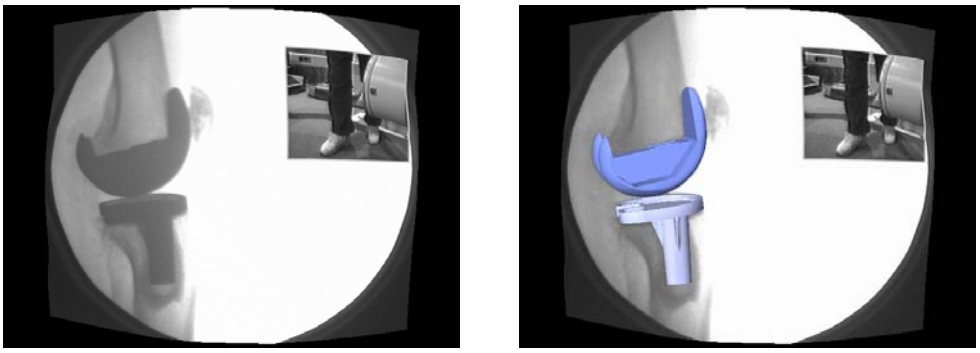

Figure 2.9: Registration of 3-D CAD models of femoral and tibial components to 2-D fluoroscopic image for a TKA subject.

2003). The rotations and translations of the rigid bodies were thus obtained from registration, and then utilized to construct the polynomial equations dependent upon θ_{flex}. For TKA knees, the implants were assumed to be rigidly fixed to the bones. This implies that the kinematics obtained of the implants were assumed to be those of the actual bones. Also, it had to be assumed that the TKA components were aligned correctly within the bones. The registration process characterizes the position of the femoral implant (or bone model, for normal knees) relative to the tibial implant by defining the position vector between the model centroids. Since it was assumed that knowledge of the actual size of the femur and tibia for both normal and TKA subjects would not be readily available, the position vector from the centroid of the 3-D CAD models to the center of mass of the bones was estimated.

The registration method estimates the femorotibial contact points by determining the closest points on the femoral condyles to the tibial plateau (Hoff et al., 1998). These points are then defined as the femorotibial contacts. The tibiofemoral contacts are then identified by drawing a vector distally in the axial tibial direction from each femorotibial point. The intersection of these vectors with the tibial plateau identifies the location of

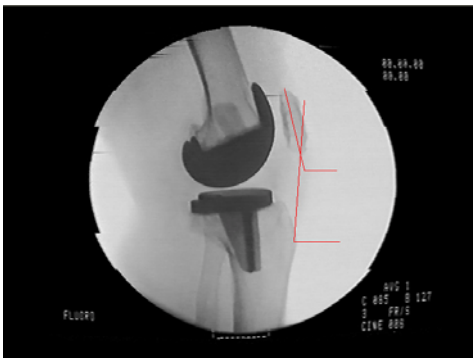

Figure 2.10: Patellar ligament and patellar tilt angle determination.

the tibiofemoral contacts. The model assumed a unicompartmental contact. The positions of the two contacts derived from the registration process were therefore averaged to minimize the error associated with the unicompartmental assumption. A single mobile contact point was thus used as the point of application of the tibiofemoral contact forces.

The patellar ligament angle, θ_{PL}, and the patellar tilt angle, sagittal patella tilt angle, θ_{Pat} (see Figure 2.6) were determined from 2-D measurements made upon the fluoroscopic image. θ_{PL} was determined by drawing a line from the tibial tuberosity to the apex of the patella. θ_{PL} was taken to be the angle between this line and the vertical. The patella tilt was approximated by drawing a line from the apex to the base of the patella. θ_{Pat} was taken to be the angle between this line and the vertical. This process is shown in Figure 2.10. Since 3-D positions of the patella were not available, both the patellar ligament and the patella were assumed to reside in the same sagittal plane as the tibia.

2.2: Application of the Model to Obtain Clinically Relevant Results

2.2.1: Normal versus TKA Tibiofemoral Forces

7 normal knee subjects (Komistek, 2003) and 7 subjects implanted with a Sigma Fixed Bearing, Posterior Stabilizing (PS) TKR (DePuy Orthopaedics, Inc; Yoshiya, 2004) analyzed from previous studies were modeled. The subjects performed a DKB under fluoroscopic surveillance from full extension to maximum flexion. Since the angle of maximum flexion varied from subject to subject, the kinematics were only obtained for full extension to 90º of flexion. Images were analyzed for the normal subjects at 15º increments, and at 30º increments for the TKA subjects. All patients signed informed consent statements, and the research was approved by both the Rose Medical Center and University of Tennessee Institutional Research Review Boards (IRRB 0445 and 897-A, respectively).

The normal group, on average, experienced normal femoral rotation, defined as external femoral rotation relative to the tibia with increasing flexion, of 18.0º from full extension to 90º of flexion. Figure 2.11 displays the average condylar rollback pattern over the DKB activity. The group had a medial pivot pattern, and achieved -21.4 mm of lateral condylar rollback and -4.2 mm of medial condylar rollback.

The TKA group experienced slight normal axial rotation from 0º to 90º of flexion of 1.1º. Figure 2.12 displays the average condylar rollback pattern for this group over the activity. The medial condylar contact achieved a minimal posterior rollback of -0.2 mm, while the lateral contact moved only slightly more posteriorly (-1.2 mm).

Axial tibiofemoral contact forces were obtained throughout the flexion cycle from the kinetic model, and the maximum contact force was recorded for each subject. Group

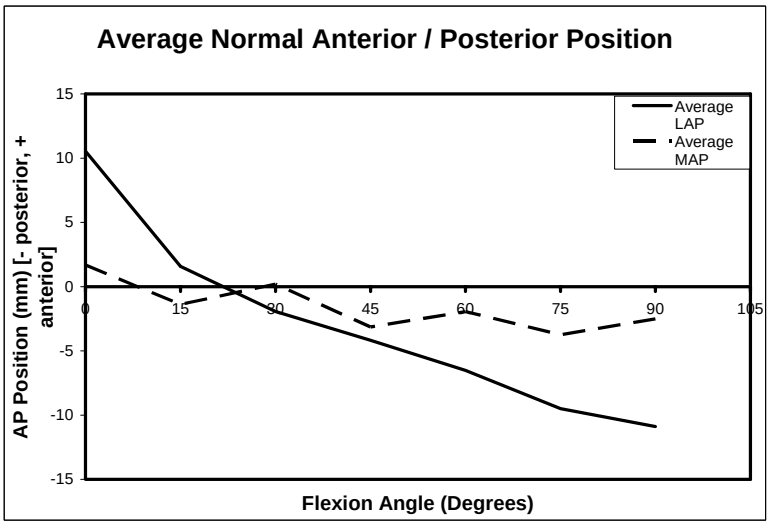

Figure 2.11: Condylar AP position over a DKB for the normal knee subjects. Zero is defined as the mid-point of the tibial plateau in the sagittal plane. Positive values represent more anterior positions.

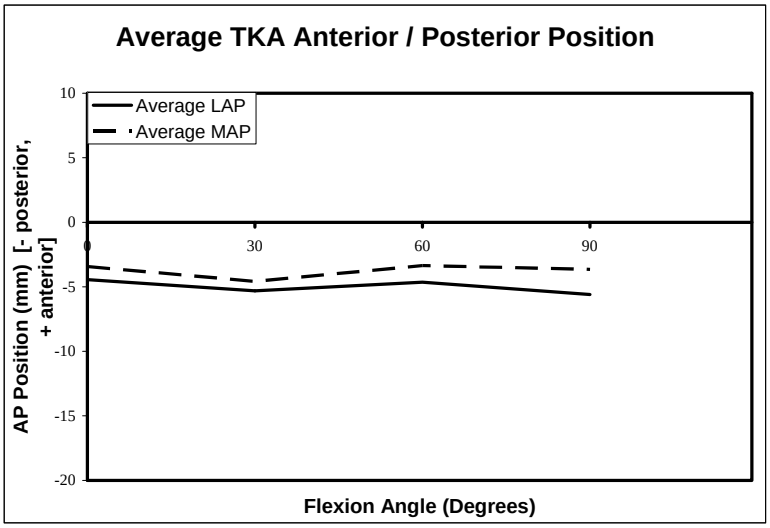

Figure 2.12: Condylar AP position over a DKB for the TKA subjects. Zero is defined as the mid-point of the tibial plateau in the sagittal plane. Positive values represent more anterior positions.

averages were obtained, and Levene's test was used to determine whether or not means could be compared assuming equal variances or not. Statistical significance was assigned at the $\alpha = 0.05$ level.

2.2.2: Kinetic Effects of Femoral Rollback

The model was adjusted for a sample subject, from the Sigma TKA group (Chapter 2.2.1) to allow for adjustment of the condylar rollback and for posterior shift of the femur relative to the tibia. This consisted of modifying the model to allow the coefficients of the polynomial parametric function for the AP position of the tibiofemoral contact to be entered into the input file. The n+1 variables $contact_0$, …,$contact_i$, …, $contact_n$, where n is the order of the polynomial, denote these coefficients. The code was also modified to allow the AP position of the femur to be entered into the input file. The subject was analyzed throughout a DKB from full extension to maximum flexion (100º). The original *in vivo* condylar contact AP positions are displayed in Figure 2.13.

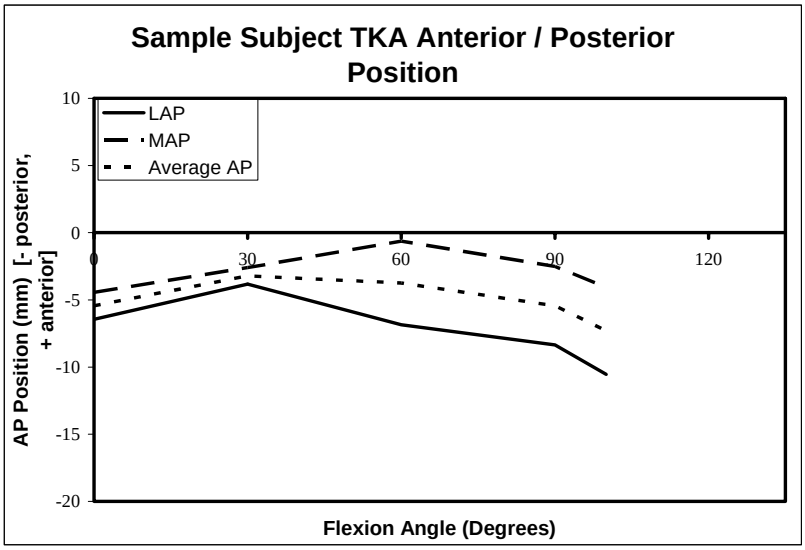

Figure 2.13: Condylar AP position over a DKB for the sample TKA subject. Zero is defined as the mid-point of the tibial plateau in the sagittal plane. Positive values represent more anterior positions.

This subject experienced -4.1 mm lateral condylar rollback, 0.4 mm anterior condylar translation, and 5.1º external femoral rotation from 0º to 100º of flexion. The average AP contact position (average of the medial and lateral contacts) demonstrated -1.9 mm of femoral rollback, or femorotibial contact translation.

The AP pattern of the average tibial condylar contact was varied over the last two increments of flexion (60º to 90º and 90º to 100º) in order to simulate magnitudes both more anterior and more posterior than -1.86 mm of femorotibial contact translation. 100º positions were input according to overall (the difference in AP position from full extension to 100 º of flexion) femorotibial contact translation values of +6 mm (6 mm anterior from the full extension position), +4 mm, +2 mm, 0 mm, -4 mm, and -6 mm. The 90º contact position was determined utilizing the same proportional distance between the 60º position and the 100º position as the original motions. Figure 2.14 displays the resulting AP positions over flexion for the various simulated AP translation patterns.

The kinetic plots were calculated for each AP pattern over the DKB activity, and the maximum tibiofemoral and quadriceps loads were tabulated for each condition. The loads were then compared with the predicted initial *in vivo* loads.

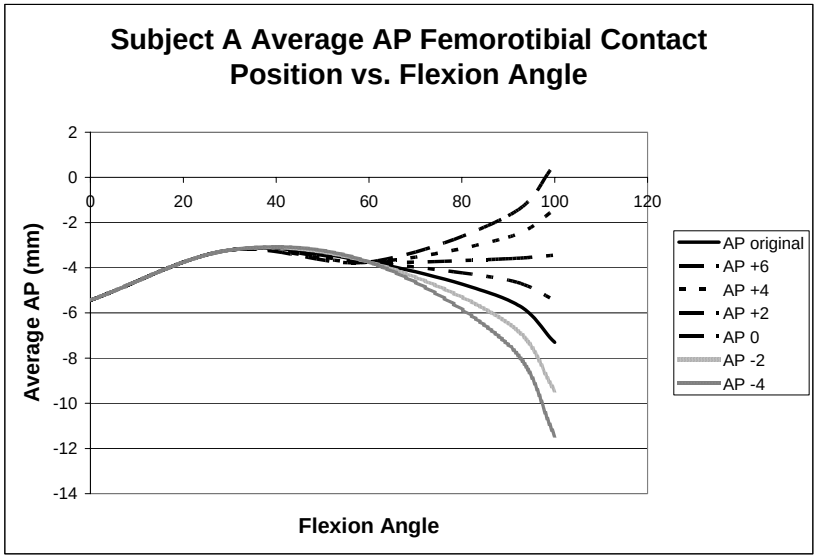

Figure 2.14: Average AP femorotibial contact patterns over a DKB for the sample TKA subject. The solid line represents the observed *in vivo* contact pattern. Overall AP translation for the activity was defined as the difference between the 100º position and the 0º position. Zero on the y-axis is defined as the mid-point of the tibial plateau in the sagittal plane. Positive values represent more anterior positions.

Chapter 3: Results

The relevant results of the constructed computational model were given by the two clinical applications of the model, since no specific results are associated with the construction of the model in general. However, in order to show the extent of the model, all calculated unknown joint forces, joint torques, soft tissue loads, ligament strains, and ligament forces are presented for a sample normal knee patient. Thus, the reported results will be confined to these three particular aspects of this study. The results are divided as follows:

3.1. Kinetic results for a sample normal knee subject

3.2. Normal versus TKA tibiofemoral forces

3.3. Kinetic effects of femoral rollback

3.1: Kinetic Results for a Sample Normal Knee Subject

The 3-D computational model of the lower limb was constructed to calculate 12 unknown forces and torques. These consist of 3 tibiofemoral forces, 2 knee torques (torques exerted by the femur onto the tibia), 3 hip joint forces, 3 hip torques (torques exerted by the pelvis onto the femur), and the patellar ligament force. All other forces included within the model were either input (the ground reaction force), dependent upon one or more of the calculated unknowns (the quadriceps force and the 2 patellofemoral contact forces), or were functions of the positions of the bones (the ligamentous forces). These results are presented for a sample normal knee subject.

The sample subject was arbitrarily chosen from a previous study (Komistek, 2003). A normal knee subject was chosen since most TKA implants involve the complete resection of one or both cruciates. When this is the case, the ligaments are not included within the model. Choosing a normal subject allowed the results for cruciate ligament forces to be demonstrated. Figure 3.1 displays the AP position of the femorotibial contacts upon the tibial plateau over the DKB at 15º increments. Zero is defined as the mid-point of the tibial plateau in the sagittal plane, with positive AP translation values denoting a position anterior to this point. Note that this subject's femur was internally rotated relative to the tibia over the majority of the DKB activity. The subject then experienced a very high amount of external femoral rotation (14.8º) in the

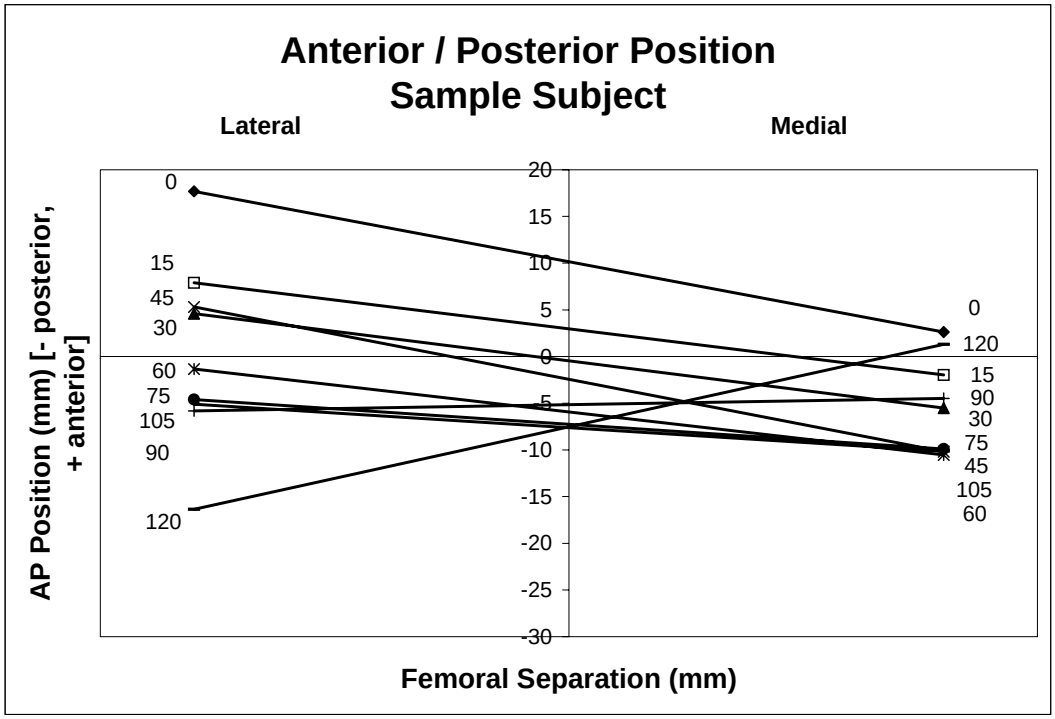

Figure 3.1: *In vivo* condylar AP positions for the sample subject. Zero, on the AP position scale, denotes the midpoint of the tibial plateau in the sagittal plane. Positive values denote positions anterior to this mid-point. The flexion angle is given for each pair of contact points.

last increment of flexion (105º to 120º). The subject experienced a total amount of external femoral axial rotation of 25.0º from full extension to maximum flexion (120º). This subject experienced 34.1 mm of lateral condylar rollback, and 1.31 mm of medial condylar rollback.

Since the flexion motion of each patient was determined from equation (2.2.1) over an interval of t = 0 to t = 1, plots were initially generated in terms of time. Figure 3.2 shows an axial tibiofemoral force plot for a sample TKA patient with respect to time. However, to obtain more clinically relevant results, plots were subsequently constructed with respect to flexion angle, θ_{flex}. Figure 3.3 gives the same tibiofemoral force profile as shown in Figure 3.2, but plotted with respect to flexion angle instead of time. It should be noted that this method resulted in some flexion dependent force plots appearing asymptotic, whereas the original time dependent plots were clearly not asymptotic.

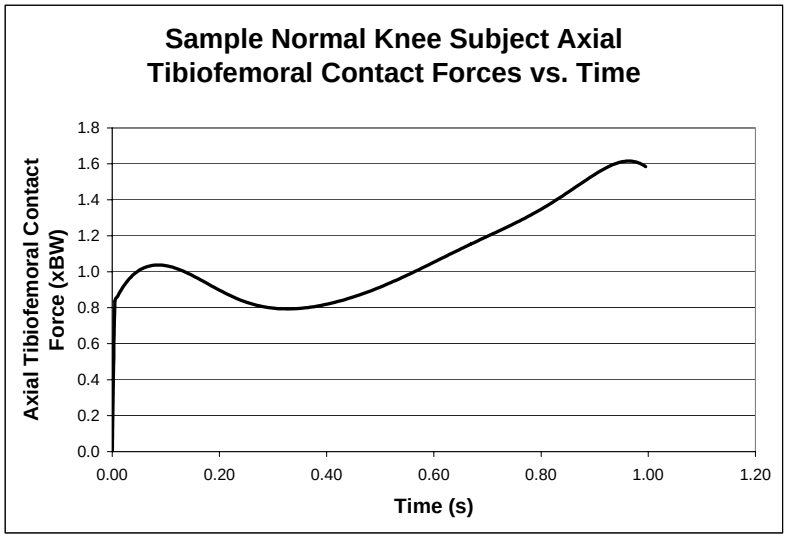

Figure 3.2: Axial tibiofemoral contact force over time for the sample normal knee patient.

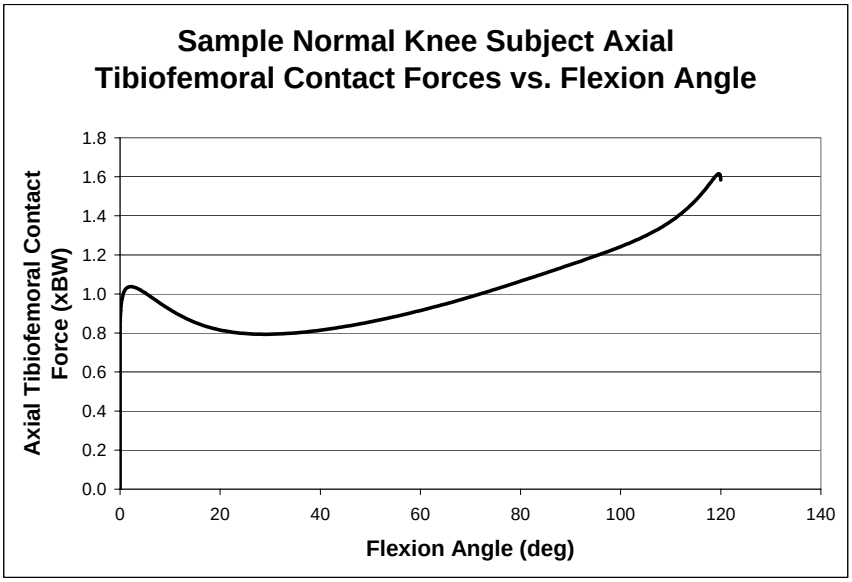

Figure 3.3: Axial tibiofemoral contact force over flexion angle for the sample normal knee patient.

3.1.1: Knee Joint Forces and Torques

The predicted tibiofemoral contact forces for the sample subject are shown in Figure 3.4. A positive AP force value indicates a posteriorly directed force exerted upon the femur by the tibia, and a positive ML force value indicates a medially directed force exerted by the tibia upon the femur. For this particular subject, the axial force peaked at 1.61xBW at about 120º of flexion. The AP force shifted from anteriorly directed to posteriorly directed at approximately 22º of flexion, and obtained a peak force of 0.75xBW at about 120º of flexion. The ML force shifted from laterally directed to medially directed at approximately 65º of flexion.

The torques exerted upon the tibia by the femur are shown in Figure 3.5. $T_{tf\text{-}1}$ represents the torque around the N_1 axis. A positive value indicates a valgus inducing torque. $T_{tf\text{-}2}$ denotes the torque around the N_2 axis. A positive value indicates a torque

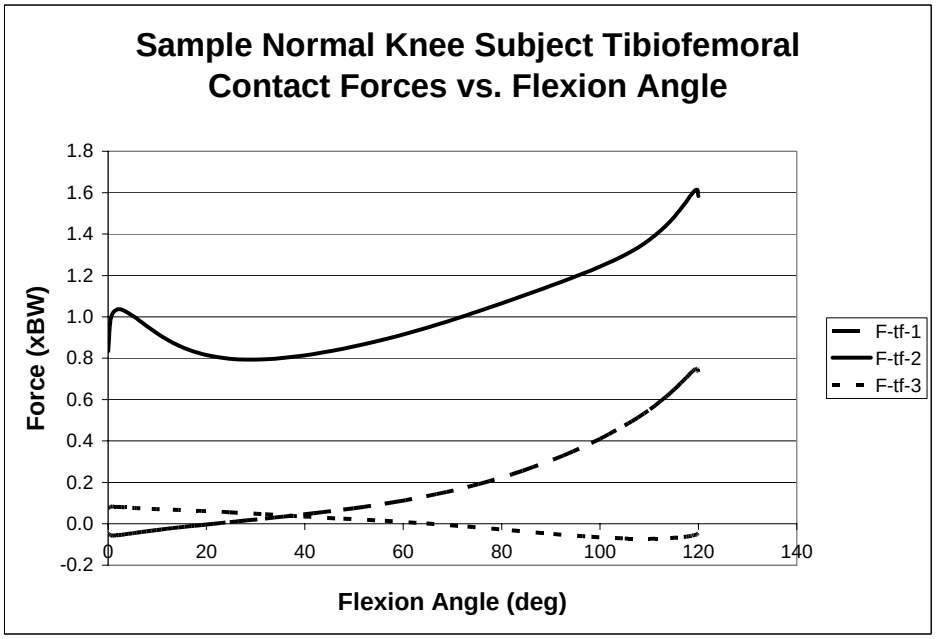

Figure 3.4: Tibiofemoral contact forces over the DKB for the sample normal knee patient. A positive $F_{TF\text{-}1}$ indicates a posteriorly directed tibiofemoral force. A positive $F_{TF\text{-}3}$ force indicates a medially directed tibiofemoral force.

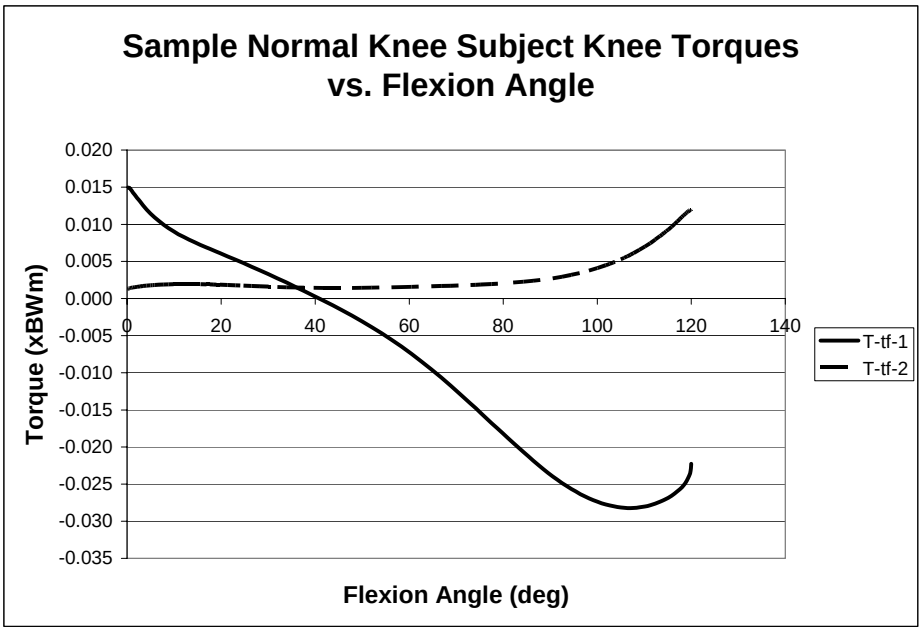

Figure 3.5: Knee torques over the DKB for the sample normal knee patient. A positive $T_{TF\text{-}1}$ value indicates a valgus inducing torque. A positive $T_{TF\text{-}2}$ value indicates an internal tibial rotation inducing torque.

inducing internal rotation of the tibia with respect to the femur. The sample patient experienced a valgus torque at the beginning of the DKB. However, at 41º of flexion, the torque changed to a varus torque. $T_{tf\text{-}2}$ remained positive over the entire activity. Both torques were very small in magnitude, with neither breaching ±0.1xBWm.

3.1.2: Patellar Forces

Predicted results for the patellar forces (see Figures 2.6 and 2.7 for diagrams) for the sample subject are given in Figure 3.6. As with the axial tibiofemoral contact force, the quadriceps force, F_Q, the normal patellofemoral force, F_{PFn}, and the patellar ligament force, F_{PL}, generally increased with flexion. Both F_Q and F_{PFn} reached a maximum of approximately 6.0xBW. A positive value of the medial-lateral component of the patellofemoral contact force, F_{PFml}, indicates a medially directed force acting upon the femur. As Figure 3.6 shows, the sample subject experienced a medially directed force

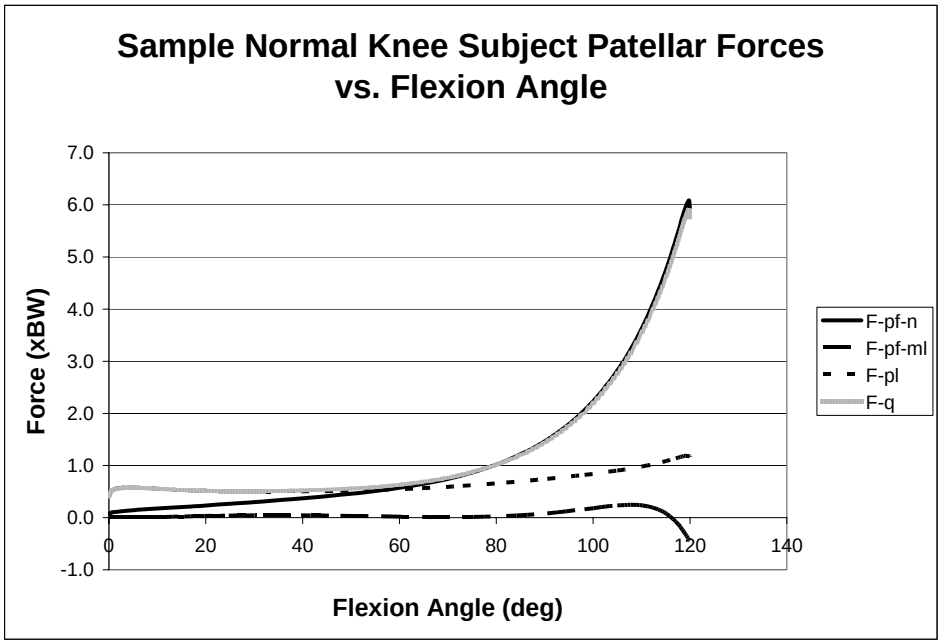

Figure 3.6: Patellar forces over the DKB for the sample normal knee patient. A positive F_{PFml} value indicates a medially directed force acting upon the femur.

over the majority of the activity, but experienced a change to a laterally directed force at 116º of flexion.

3.1.3: Hip Joint Forces and Torques

Calculated hip joint forces exerted by the pelvis onto the femur are displayed in Figure 3.7 for the sample subject. A positive value of the AP component, F_{H-1}, represents a posteriorly (in the pelvic, or global, reference frame N) directed force acting upon the femur. A positive SI component, F_{H-2}, represents a downward force in the direction of gravity. A positive ML component, F_{H-3}, indicates a medially directed force (relative to the pelvis) acting upon the femur. As Figure 3.7 demonstrates, F_{H-1} generally wavered around 0xBW throughout the activity. The downward force followed a similar pattern as the ground-reaction force (Figure 2.4). F_{H-3} acted in a medial direction until

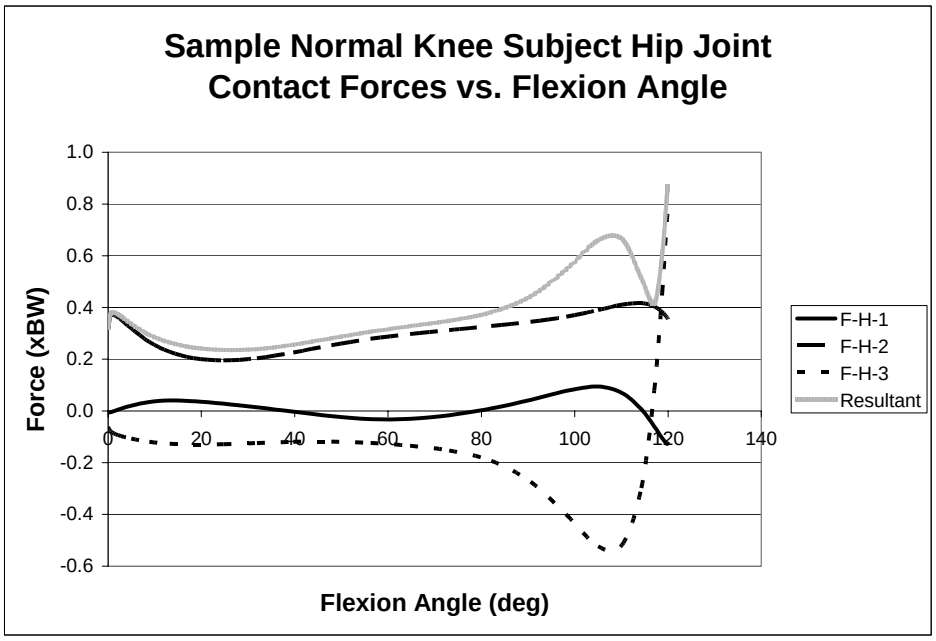

Figure 3.7: Hip joint reaction forces over the DKB for the sample normal knee patient. A positive F_{H-1} value indicates a posteriorly directed force acting upon the femur. A positive F_{H-2} value indicates a downward force. A positive F_{H-3} value indicates a medially directed force upon the femur.

approximately 116º of flexion, after which it acted in a lateral direction. This phenomenon was also observed in the ML patellofemoral contact force pattern for this subject, as shown in Figure 3.6.

The torques exerted by the pelvis onto the femur are shown in Figure 3.8. A positive value for the torque in the N_1 direction, T_{H-1}, indicates an abduction moment upon the femur. A positive value for the torque in the N_2 direction, T_{H-2}, indicates a moment internally rotating the femur relative to the pelvis. A positive value for the torque in the N_3 direction acts to cause extension of the femur relative to the pelvis. The three torques were less than 0.1xBWm over most of the DKB. However, after approximately 112º of flexion, the torques rose in magnitude, with T_{H-2} reaching a maximum of 0.69xBWm.

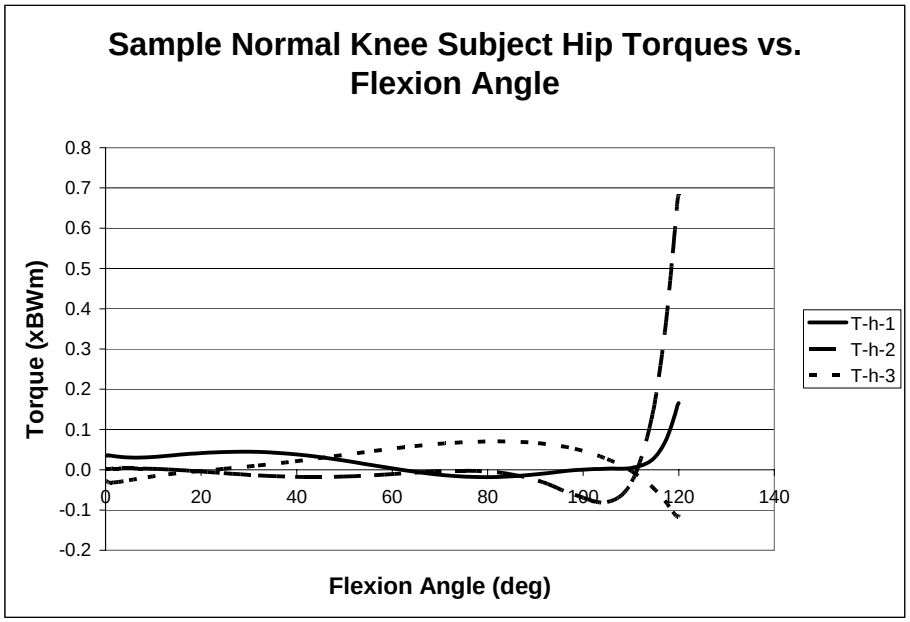

Figure 3.8: Torques exerted by the pelvis onto the femur over the DKB for the sample normal knee patient. A positive T_{H-1} value induces femoral adduction. A positive T_{H-2} value induces internal rotation of the femur relative to the pelvis. A positive T_{H-3} value induces extension of the femur relative to the pelvis.

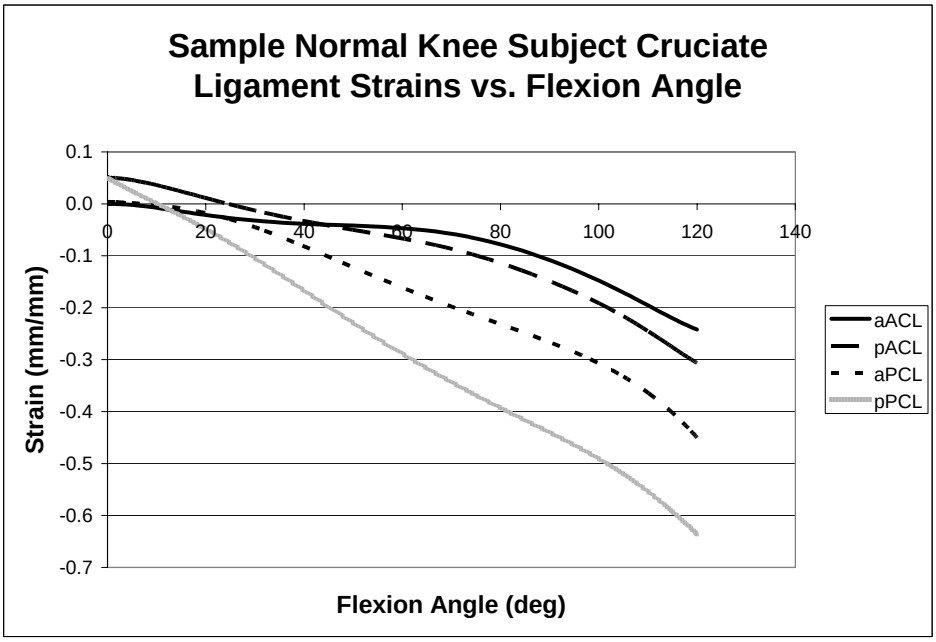

Figure 3.9: Cruciate ligament strains over the DKB for the sample subject.

3.1.4: Ligamentous Strains and Forces

The ligamentous forces were functions of the ligament strain, as defined by equations (2.2.12) and (2.2.13). The strains for the cruciate ligaments over the DKB are given in Figure 3.9, and those for the collateral ligaments are given in Figure 3.11. All four bundles of the cruciates decreased in length over the DKB. The LCL decreased in length over the DKB as well. All three bundles of the MCL initially increased in length, then gradually decreased. The deep bundle of the MCL was the only bundle to have a strain greater than 0 over the entire activity. The corresponding cruciate and collateral ligament forces are shown in Figure 3.10 and 3.12, respectively. Only the posterolateral ACL bundle and the posteromedial PCL bundle produced notable cruciate forces, and both had decreased to 0 by 30º of flexion. The posterolateral ACL bundle peaked at 0.017xBW (approximately 12.9 N) and the posteromedial PCL bundle achieved a maximum force of

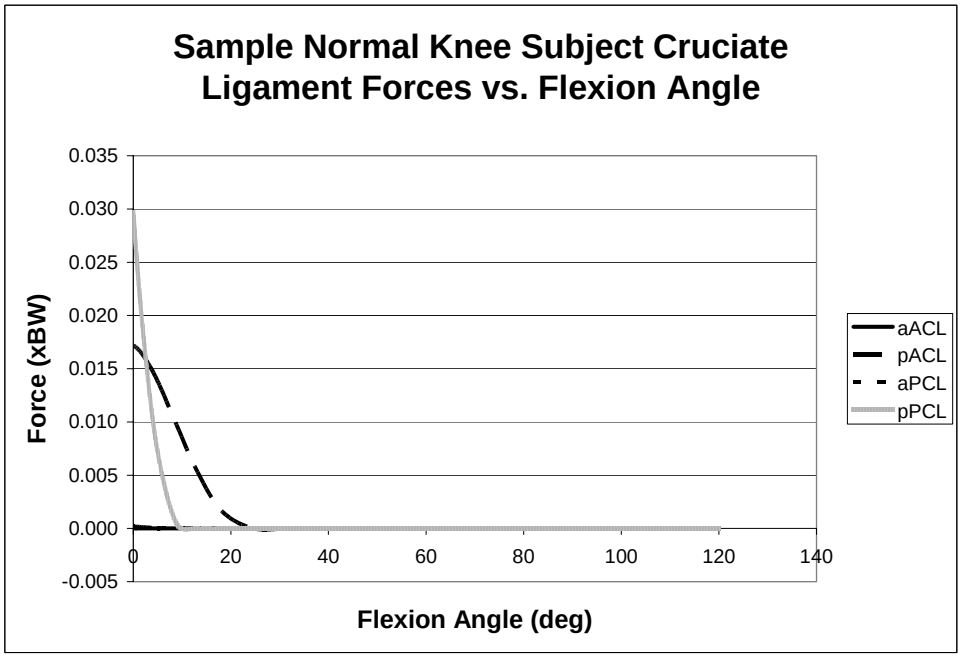

Figure 3.10: Cruciate ligament forces over the DKB for the sample subject.

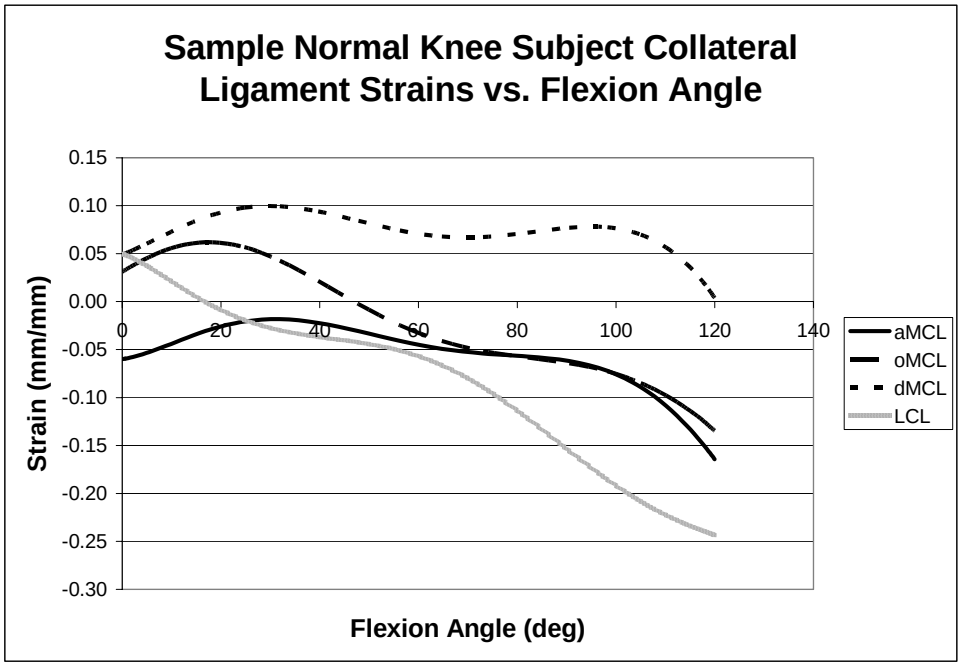

Figure 3.11: Collateral ligament strains over the DKB for the sample subject.

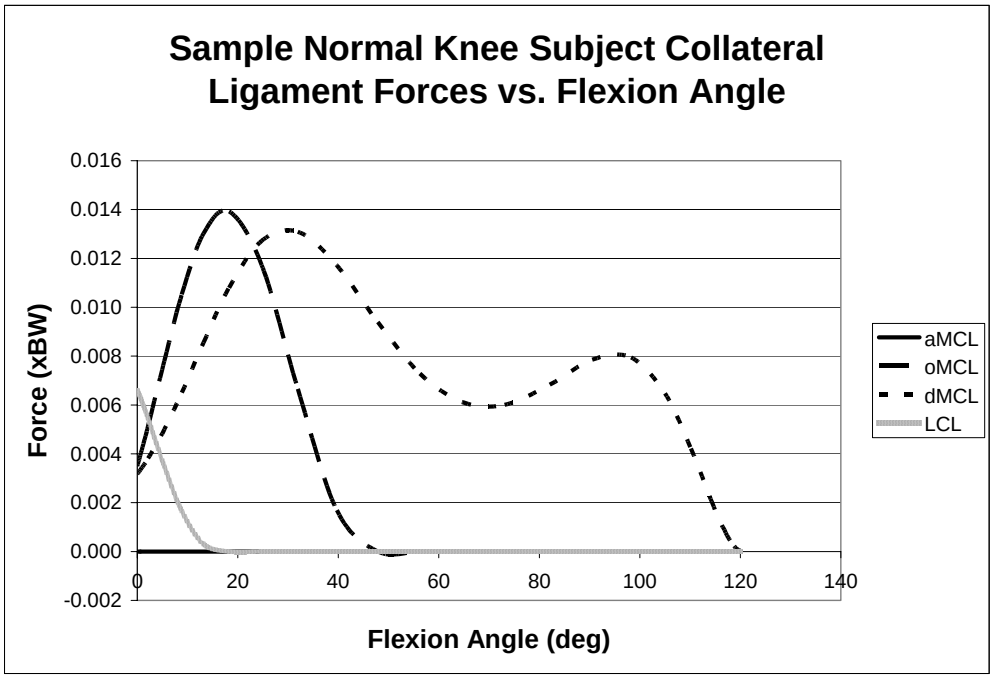

Figure 3.12: Collateral ligament forces over the DKB for the sample subject.

0.030xBW (22.7 N). The peak LCL force was 0.007xBW (5.3 N), occurring at full extension. The anterior MCL bundle did not significantly contribute, while both the oblique and deep bundles exhibited an initial increase in force to 0.014xBW (10.6 N) at 16º of flexion and 0.013xBW (9.8 N) at 29º of flexion, respectively.

3.2: Normal Versus TKA Tibiofemoral Forces

Axial tibiofemoral contact forces were determined over the DKB activity from full extension to 90º of flexion for each of the 14 subjects (7 normal knee and 7 TKA). For all subjects, the general pattern of the force was to increase over the DKB activity, similar to the normal knee sample subject pattern shown in Figure 3.4. The maximum force was generally achieved near 90º flexion. The normal subjects achieved a mean maximum axial tibiofemoral force of 1.35xBW (maximum = 1.70xBW, minimum =

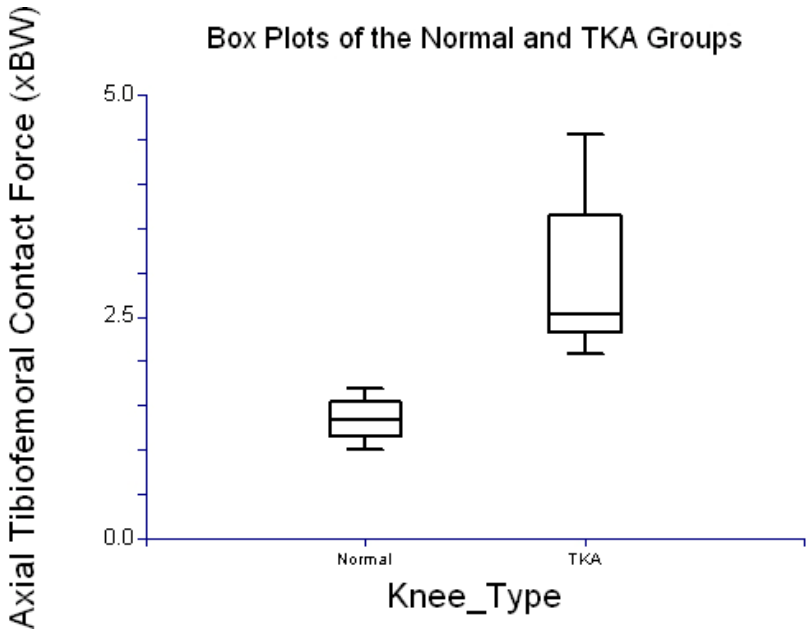

Figure 3.13: Box and whiskers plot of the axial tibiofemoral contact forces for both the normal and TKA groups.

1.00xBW, standard deviation (σ) = 0.236xBW). The TKA subjects achieved a mean maximum force of 2.99xBW (maximum = 4.56xBW, minimum = 2.09xBW, σ = 0.889xBW). Figure 3.13 displays a box and whiskers plot for the two groups. The TKA distribution is much larger than the normal group (as also evidenced by the larger standard deviation). The TKA distribution is also skewed to the right, whereas the normal knee distribution is mostly symmetric.

The variances of the two groups were compared using Levene's test, which concluded that the variance of the TKA group was significantly higher than the normal knee group ($p = 0.0064$). Since the variances were not equal, a standard t-test could not be used to compare the means of the two groups. A Welch comparison of means (also known as the Welch-Satterthwaite method [Tamhane and Dunlop, 2000]), assuming

unequal variances, was performed in order to compare means. The TKA group experienced a significantly higher axial tibiofemoral contact force than the normal knee group ($p = 0.0023$). A nonparametric Kruskal-Wallis ranked sum test was performed in order to verify this conclusion, since the TKA distribution appeared to deviate from normality slightly. However, this test indicated that the TKA groups experienced a significantly higher force than the normal group with the same certainty ($p = 0.0023$).

3.3: Kinetic Effects of Femoral Rollback

Axial tibiofemoral force and quadriceps load profiles were generated for each AP femoral translation condition, and maximum values were tabulated. The original force profiles, prior to adjusting the AP position of the femorotibial contact, are displayed in Figure 3.14. The predicted maximum axial tibiofemoral contact and quadriceps forces were 2.32xBW and 3.59xBW, respectively. The maximum values for each simulated AP

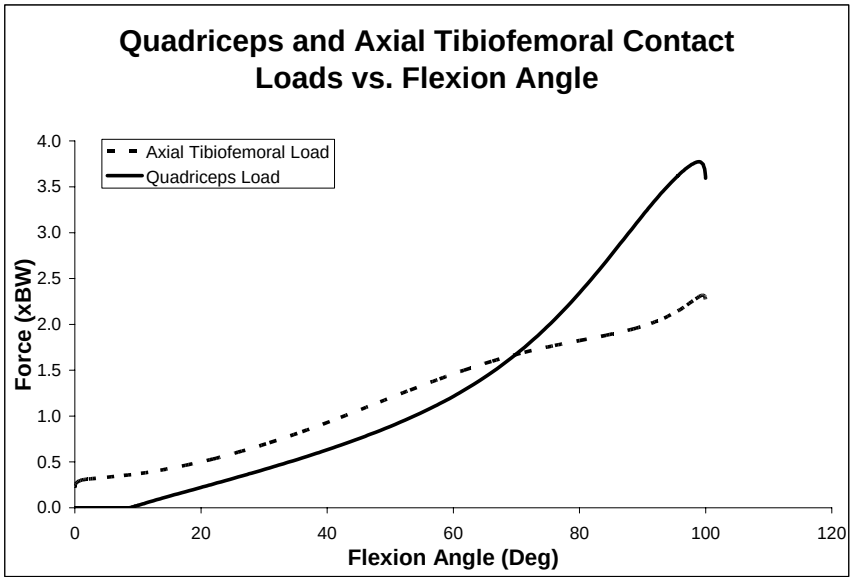

Figure 3.14: The calculated axial tibiofemoral contact force and quadriceps load for the naturally occurring kinematics of the sample subject.

Table 3.1: Maximum tibiofemoral and quadriceps loads for each simulated shift of the femorotibial contact. Percent differences are relative to the original in vivo kinematics (-1.86 mm of AP). Translation values represent the difference in AP position between the 100º flexion and the full extension positions. Positive translations indicate an anterior translation upon the tibial plateau.

Femorotibial Contact AP Translation	Tibiofemoral Contact Load	% Difference	Quadriceps Load	% Difference
+6 mm	2.84	22.45 %	4.57	27.14 %
+4 mm	2.69	16.14 %	4.30	19.72 %
+2 mm	2.53	9.01 %	4.00	11.21 %
0 mm	2.41	4.08 %	3.78	5.16 %
-1.86 mm	2.32	0 %	3.59	0 %
-4 mm	2.22	-4.21 %	3.40	-5.46 %
-6 mm	2.11	-8.97 %	3.17	-11.84 %

translation condition are given in Table 3.1. The maximum axial tibiofemoral contact force is plotted in Figure 3.15 against the amount of AP femorotibial contact translation from full extension to 100º of flexion. By shifting the maximum flexion femorotibial contact position 6 mm anteriorly to the full extension position, the contact force increased 22.45% to 2.84xBW. A posterior translation of -6 mm resulted in a decrease of 8.97% to 2.11xBW. Figure 3.16 displays the analogous plot for the quadriceps force. An anterior femorotibial contact translation of 6 mm corresponded to a 27.14% increase in quadriceps force to 4.57xBW. A posterior translation (or rollback) of 6 mm resulted in a 11.84% decrease to 3.17xBW. The quadriceps and contact load profiles over the various translation conditions followed similar trends, although the quadriceps load experienced greater differences in magnitude in response to translation adjustments.

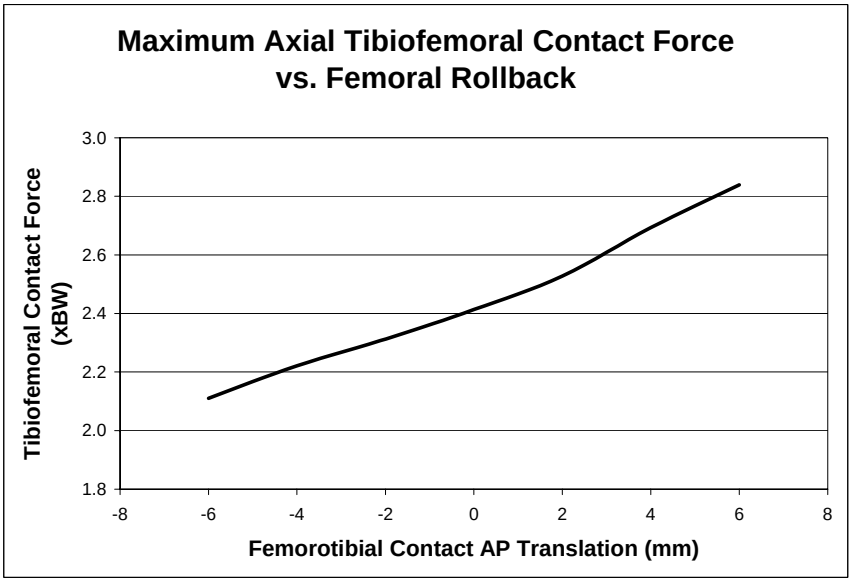

Figure 3.15: Maximum axial tibiofemoral contact force plotted against the different AP translation conditions for the femorotibial contact. Translation values represent the difference in AP position between the 100º flexion and the full extension positions. Positive translation values indicate an anterior translation upon the tibial plateau.

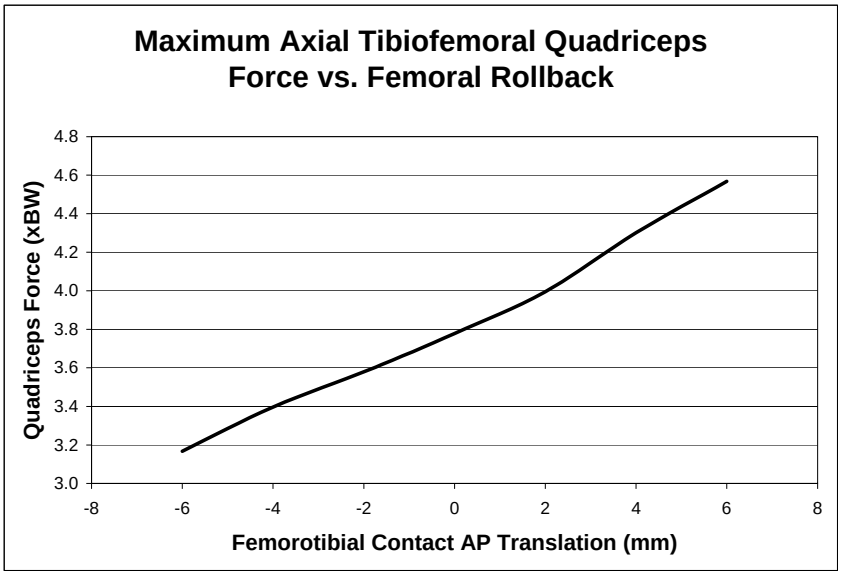

Figure 3.16: Maximum quadriceps force plotted against the different AP translation conditions for the femorotibial contact. Translation values represent the difference in AP position between the 100º flexion and the full extension positions. Positive translation values indicate an anterior translation upon the tibial plateau.

Chapter 4: Discussion

A computational model was constructed to predict 3-D *in vivo* lower limb dynamics from input kinematics obtained fluoroscopically. The inverse dynamics model utilizes a reduction approach to simplify the statically indeterminant lower limb system. Results were presented for a sample normal knee subject undergoing a DKB. The model was then applied to two clinically relevant sub-studies. Firstly, the model was used to compare the axial tibiofemoral contact forces between 7 normal knee subjects and 7 TKA subjects. Secondly, the model was used to evaluate the kinetic effects of femoral rollback.

The results presented for the sample patient serve mainly to demonstrate the capabilities of the computational model, and to provide an example of all possible loads that can be predicted by the model. Since sample statistics cannot be obtained from one patient, and thus population parameters should not be estimated, the actual values of the sample subject should not be generalized to all knees. Results varied according to different input kinematics. Therefore, since kinematics differs from subject to subject, force profiles from one subject cannot be generalized to all. Also, many previous studies that predicted *in vivo* kinetics or experimentally determined in vitro kinetics failed to incorporate realistic kinematics. Thus, differences between the output kinetics and those reported in the literature should always be expected. Minor or occasional disagreements with the literature should not be taken as evidence that the computational model is faulty. Nevertheless, the sample results can be used to verify that the model is within reason.

Comparisons to previous studies are difficult due to the lack of DKB activities being included in telemetric and mathematical analyses. However, comparisons to gait

and stair ascending, when available, were assumed to provide some illumination upon the validity of this model. It should be noted that the stance phases of both gait and stair ascending require one leg to support the entire upper body. A DKB allows the body weight to be distributed between both legs, although the force-plate data in Figure 2.4 indicates that most of the weight is indeed on the target leg at high flexion angles. Also, during gait and stair ascending, the ground contact is generally either anterior or posterior to the mass center of the body, especially near heel-strike and toe-off. Due to the lack of forward momentum, the mid-point between the two ground contacts throughout a DKB is likely directly beneath the body mass center. This would result in less of a moment around joints, particularly around the flexion-extension axis of the hip. For these reasons, it was expected that the kinetic results from the model, particularly joint moments and hip forces, would be slightly less than previously reported data in the literature. Indeed, for a telemetric study, peak hip contact forces for a knee bend have been found to be 55.5% to 71.4% to those obtained for normal walking, and 51.5% to 66.8% to those obtained for stair ascending (Bergmann et al., 2001).

The model generated knee reaction loads comparable to previous telemetric and mathematical studies, indicating that this modeling approach is both reliable and relevant. A previously conducted subject specific approach obtained axial knee forces in the range of 1.7 to 2.3 BW during gait for a normal knee subject (Komistek et al., 1998). The corresponding peak axial knee force for the sample subject undergoing a DKB in this study was 1.6xBW, which is similar in magnitude. Furthermore, a study utilizing telemetry obtained average distal femoral shaft forces of 3.1 and 2.8 BW for stair descending and stair ascending, respectively, which, although is likely to cause higher

axial forces, is the closest activity to DKB that was analyzed (Taylor and Walker, 2001). The peak axial knee force of 1.6xBW obtained here thus seems reasonable. Also, the distal femoral shaft subjects had been implanted with a rotating hinge knee, which may be responsible for higher axial loads, as will be discussed shortly.

As demonstrated in Figure 3.8, the peak AP torque exerted by the femur on the tibia was -2.8xBWcm, i.e., the knee joint peak AP torque was 2.8xBWcm (varus inducing). The peak predicted SI torque was 1.2xBWcm, acting to internally rotate the tibia. Taylor and Walker measured peak AP varus moments of 6.9-9.0xBWcm during a stair ascending activity from distal femoral telemetry (2001). Since stair ascending would be expected to generate higher AP torques than a DKB due to the increased weight on the leg, the values generated seem reasonable. Similarly, Taylor and Walker measured peak SI moments of -0.4-1.3xBWcm during stair ascending. The values predicted by the computational model are similar in magnitude, but acting in the opposite direction. This could possibly be due to the difference in body movement between a DKB and stair ascending. However, the model predictions are definitely within reason.

As expected, hip reaction loads were smaller than those reported from previous mathematical and telemetric analyses for gait and stair ascending. Rydell reported hip joint forces of about 1.6xBW during normal gait, as determined from a telemetric hip prosthesis (1965). However, it was noted that slower gait resulted in lower hip forces. Very slow gait actually resulted in a resultant hip force of less than 1.0xBW, implying that the speed of the DKB should be accounted for when comparing to previous studies. An optimization technique, solving 33 unknowns with 8 equations, revealed a resultant hip force of 3.3-5xBW during gait, and greater than 7xBW during stair ascending

(Crowninshield, 1978). A telemetric proximal femoral prosthesis was used to obtain femoral shaft forces of greater than 3.0xBW during stair ascending, which is theoretically only a 3-9% difference between the hip resultant force (Taylor et al., 1997). Although, these studies generated forces notably higher than those generated by the computational model, a telemetric hip prosthesis was used to obtain peak hip resultant forces of 1.17-1.77xBW over a knee bend. This is much closer to the peak resultant load of 0.87xBW (Figure 3.8) generated by the sample subject. Additionally, preliminary results for a mathematical model of the hip have been presented (Alford et al., 2005), and future incorporation with this model may lead to a much more accurate lower limb model.

The predicted torques across the hip joint were similar in magnitude to previously reported data. Crowninshield et al. found peak moments of approximately 0.12xBWm, 0.015xBWm, and 0.074xBWm for T_{H-1}, T_{H-2}, and T_{H-3}, respectively, during gait (1978). The corresponding peak torques obtained here were 0.17xBWm, 0.69xBWm, and 0.07xBWm. These are in very good agreement with Crowninshield et al., except for the notably large value for T_{H-2}. The apparent cause for this was the extreme amount of external femoral rotation (14.8º) for the subject in the last 15º of flexion (Figure 3.1).

Most previously published literature containing estimations of *in vivo* quadriceps, patellofemoral, and patellar ligament loads do not apply to weight-bearing activities, particularly a DKB. Additionally, there is wide variability amongst the data that has been reported. Li et al. used an optimization based computational model to predict quadriceps forces of 4.0-5.0xBW during a weight-bearing isokinetic flexion/extension exercise (1999a). These results are comparable to that obtained for the sample subject (6.0xBW). Singerman et al. utilized a load frame to simulate a squatting motion in cadaver legs and

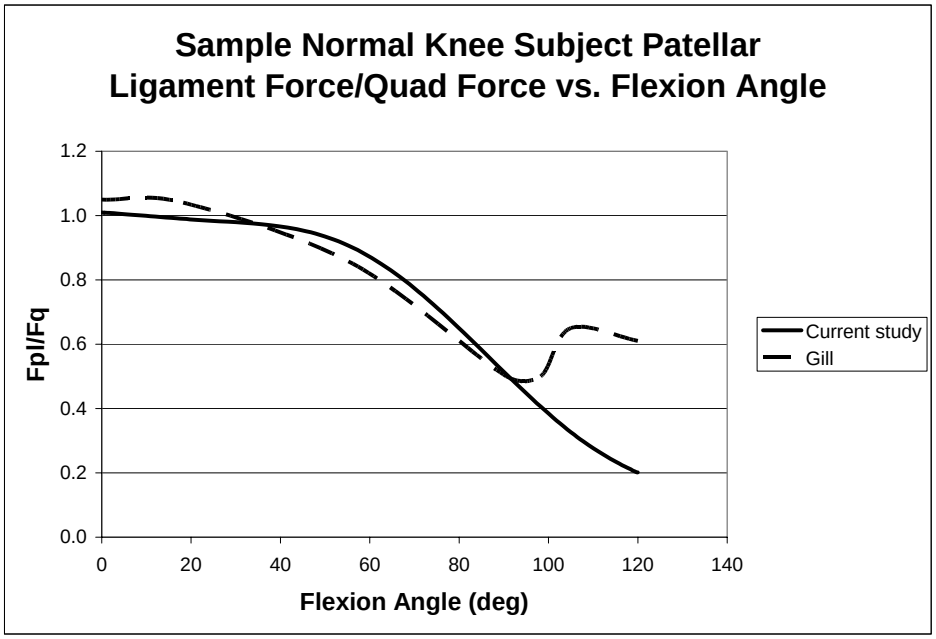

Figure 4.1: The ratio F_{PL}/F_Q plotted against flexion angle for this study and for a previous mathematical model (Gill and O'Connor, 1996).

found a maximum quadriceps force of approximately 0.6xBW (1999). However, the only applied load utilized in the simulation consisted of the leg weight and articifical hip joint. Halloran et al. used the Purdue knee simulator to measure the quadriceps force during simulated gait of two cadaveric knees (2005). The peak force was approximately 1.8-2.0xBW. These forces are less than those obtained here, but as evidenced in Figure 3.1.6, the quadriceps force did not breach 2.0xBW until 98º of flexion. Hence, gait forces, occurring when flexion is generally less than 98º, would be comparable to those of Halloran et al. In addition to the limited availability of previous data with which to compare the results obtained here, many authors have presented forces in ratio form rather than in force values. Figure 4.1 displays the ratio of F_{PL} to F_Q over the DKB activity for the results generated by this model and those generated by a previous model based off of a 4-bar linkage ligament system (Gill and O'Connor, 1996). Although the

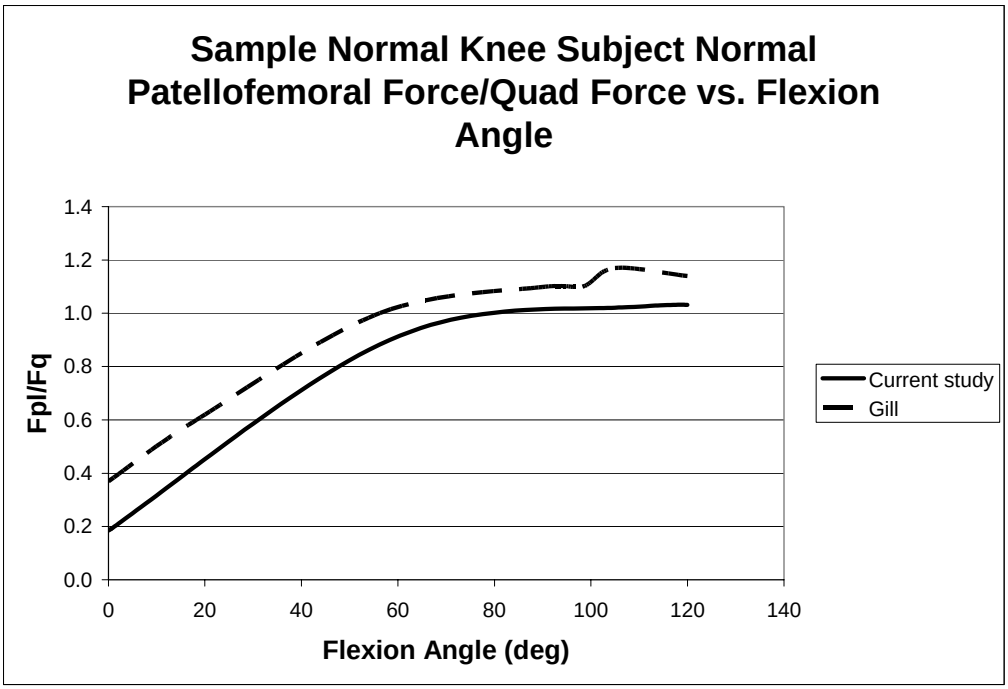

Figure 4.2: The ratio F_{PFn}/F_Q plotted against flexion angle for this study and for a previous mathematical model (Gill and O'Connor, 1996).

previous model was only 2-D, the ratios are very similar. The discrepancy above 90º of flexion is likely due to the fact that this model did not incorporate soft-tissue wrap around of bone. Similarly, Figure 4.2 displays the ratio F_{PFn}/F_Q over flexion for both this model and that of Gill and O'Connor. Again, the plots are very similar, with that of Gill and O'Connor being slightly higher in magnitude.

The literature is full of contradictions and varied results regarding ligament mechanics over flexion, but the strains observed in the sample subject are consistent with many of the reported observations. As demonstrated in Figures 3.9 and 3.11, the LCL and all bundles of the ACL and PCL decreased in length over the DKB for the sample subject. The LCL has consistently been shown to exhibit this decrease in length over flexion (Wang and Walker, 1973; Burks, 1990; Harfe et al., 1998). Results are more

varied with the cruciates, but some do agree with this decrease in length. Wang and Walker found an overall decreasing pattern in the PCL with flexion, without considering separate bundles, in cadaveric knees (1973). Using magnetic resonance imaging (MRI) and fluoroscopy, Li et al. found a decreasing length pattern in both bundles of the ACL over flexion for a lunge activity (2004). However, an increase in PCL length was found with increasing flexion. Also, Burks summarized that the anteromedial bundle of the ACL increases with flexion while the posterolateral bundle decreases. Likewise, he summarized that the posteromedial bundle of the PCL relaxes with flexion while the anterolateral bundle becomes more taut (1990). Consistent with the data obtained here, Harfe et al. found an increase of the MCL to 45º of flexion, followed by a consistent decrease to 120º of flexion (1998). However, Wang and Walker observed decreasing MCL length over flexion (1973).

The ligament forces calculated for the sample subject were generally lower than those reported in the literature. Toutoungi et al. used a gait analysis-based 2-D mathematical model to predict increasing PCL forces and no ACL forces during a descending squat (2000). However, the PCL forces peaked at approximately 2000 N, which exceeds the reported PCL tensile strength of 739 N (Trent et al., 1976) to 1051 N (Kennedy, 1976). Mommersteeg et al. utilized a RSA-based mathematical model to predict PCL forces of approximately 10 N at full extension, followed by no PCL loading throughout the rest of flexion (1997). This is very similar to the pattern for the posteromedial PCL bundle (22.7 N at full extension, decreasing to 0 N by 30º of flexion) obtained here. However, Mommersteeg et al. also obtained peak ACL loads of approximately 130 N, much greater than that obtained here (12.9 N). This was likely due

to this subject's generally anterior position of the femur relative to the tibia throughout the activity (Figure 3.1), which would have reduced ACL tension. Shelburne and Pandy used a 2-D mathematical model to predict aACL, pACL, aPCL, and pPCL forces of approximately 230 N, 310 N, 260 N, and 70 N (1997). Although these forces drastically exceed those for the sample subject, they were calculated for a simulated isometric extension activity at different flexion angles, which could easily affect the AP position of the femur relative to the tibia. Abdel-Rahman et al. used a 3-D mathematical model to predict knee kinetics, and found peak aMCL, oMCL, dMCL, and LCL forces of approximately 90 N, 30 N, 130 N, and 93 N, respectively (1998). Although these forces are much larger than those obtained here, they were in response to a sinusoidal anterior load applied to the tibia at different flexion angles. This would expectantly increase the ligament loads. The ligament loads obtained here appeared to be reasonable, although studies on *in vivo* collateral loads during weight-bearing flexion are relatively scarce.

Regarding the normal knee versus TKA knee study, the predicted tibiofemoral forces were higher in TKA subjects than in the normal subjects. There were two apparent causes for this phenomenon: the greater magnitudes of femoral rollback in the normal group (Figures 2.10 and 2.11), and the abscence of the cruciate ligaments in the TKA group. Subjects with greater rollback generally had smaller contact loads, attributed to the larger moment arm of the quadriceps. In the abscence of the cruciate ligaments, the quadriceps load increased in order to compensate for the lack of stabilizing forces. This resulted in larger contact forces.

Although higher than normal flexion-extension moments have been observed in TKA subjects, particularly those with non-anatomical designs (Andriacchi et al., 1997),

the author is unaware of any prior study using a 3-D computational model to show higher axial tibiofemoral loads in TKA knees than in normal knees. The literature is full of studies that have utilized simulators or finite element (FE) models to predict polyethylene stresses, wear rates, and failure mechanisms at various flexion angles. Most of these utilize a constant load to simulate body weight over the entire flexion range (Hsu and Walker, 1989; Essinger et al, 1989; D'Lima et al., 2001c; Liau et al., 2002; Coughlin et al., 2003; D'Lima et al., 2003). Other studies are vague regarding either the utilized loading conditions or the exact methods of how they were obtained (Bristol et al., 1996; D'Lima et al., 2001a). A few studies have utilized parametric force plots over the course of an activity, but these force profiles are often based upon normal knee kinetics (Walker et al., 1997; D'Lima et al., 2001; Miura et al., 2002; Taylor and Barrett, 2003). The results obtained from this computational model indicate that these studies may not model knee dynamics accurately. The potential higher forces in TKA knees would generate higher stresses, and thus higher polyethylene wear rates, than those measured from experiments based upon normal knee kinetics. Additionally, studies utilizing a constant load oversimplify the conditions. The axial force profiles from this study indicated that the lowest forces generally occurred at or near full extension, and the greatest forces near maximum flexion (for example, as demonstrated in Figures 3.4 and 3.14). It is of both clinical interest and design interest to know what angles of flexion generate the lowest and highest stresses. Applying a constant load over an entire activity prevents these results from being obtained. This study indicates that more accurate stresses and dynamics can be predicted by utilizing parametric force profiles, specific to both the activity and the type of knee (normal versus TKA) being considered.

The second application of the model, evaluating the kinetic effects of variations in AP femorotibial translation, determined that increasing femoral rollback led to improve knee kinetics, characterized by a decrease in both the quadriceps load and the axial tibiofemoral contact force. A difference of 12 mm (6 mm rollback to 6 mm anterior translation, or "rollforward") in AP femorotibial translation led to differences of 0.7xBW and 1.4xBW in the axial tibiofemoral force and the quadriceps load, respectively (Table 3.1). Numerous studies have assessed the occurrence of femoral rollback both in vitro (Li et al., 2001; Most et al., 2003) and *in vivo* (Dennis et al., 1996; Nozaki et al., 2002). In vitro studies have shown that rollback improves range of motion and has been shown to cause a decrease in the quadriceps load (Mahoney et al., 1994) and patellofemoral contact force (Churchill et al., 2001). Additionally, FE analyses have demonstrated a reduced patellofemoral contact force for increased rollback and an increase in contact force for increased anterior translation (D'Lima, 2003). To the author's knowledge, the current study is the first to attempt to quantify the *in vivo* kinetic effects of varying femoral rollback. The reduced axial loading associated with increased rollback implies that TKA patients that experience greater rollback may exhibit lower wear rates and longer implant lifetimes. Additionally, due to the greater quadriceps efficiency, increased rollback may be associated with quicker rehabilitation rates for patients in which the extensor mechanism has been disrupted.

The two applications undertaken in this study have direct knee design implications when viewed together. Firstly, higher flexion angles correspond to higher axial tibiofemoral contact loads. Secondly, decreased femoral rollback and anterior femoral translation also result in higher axial tibiofemoral contact loads. There is a

current industrial trend to design TKA implants that will accommodate high angles of flexion. This study indicates that this will increase the axial loads within the implant. Also, if the designs to not encourage rollback and if the patient has high laxity within the joint space, then there is potential for the femur to anteriorly translate on the tibia. This would create a very hazardous situation for the polyethylene component, as well as the fixation interfaces, due to two factors combining to increase the axial load. This study gives quantitative evidence to show that it is of prime importance for design engineers to ensure that femoral rollback will occur in these high flexion TKA designs.

This computational model does have limitations that should be noted. The geometrical bone properties, segment inertial properties, and soft tissue attachment sites were taken from population studies available in the literature. Subject specific MRI data provides a much better, and possibly the best, option for obtaining these parameters. As previously stated, the ground-reaction force was not available for most subjects in this study. Since subjects exhibit differences in how they perform the DKB, the most accurate method would be to collect subject specific ground reactions. This model does not incorporate muscle or ligament wrap-around (of bony structures), a phenomenon that has been incorporated into several previous mathematical models (Hefzy and Grood, 1983; Shelburne and Pandy, 1997; Li et al., 1999b). This phenomenon mostly affects the quadriceps at angles of flexion above approximately 88º (Gill and O'Connor, 1996), and the MCL and PCL at all times. The model assumes a unicompartmental tibiofemoral contact. This was done for computational stability, but clearly oversimplifies the joint. Incorporating both the medial and lateral contacts into the model would allow for comparisons between the contact forces due to phenomena such as condylar lift-off,

increased varus/valgus torques, TKA component malalignment and malrotation, and medial osteoarthritis. The input temporal flexion function was identical for all subjects, as previously discussed. This was done to eliminate misleading differences in kinetics due to subject variations in the speed with which the activity was performed. However, to obtain truly accurate results, the actual motion of the subjects should be used, and the speed with which the activity is performed should be standardized at the time of data acquisition. This will minimize the possibility of erroneous conclusions being drawn due to differences in subject speed, yet will allow the calculation of the most realistic results. Finally, there has been much effort in the literature to standardize coordinate systems in order to avoid "kinematic cross-talk." This model currently utilizes the reference frames embedded in the non-commercial 3-D registration software. The femoral and tibial reference frames are established based upon a CAD model bounding-box, that is, a rectangular prism completely surrounding the CAD model. For TKA implant models, this is fairly standardized. However, for normal bones constructed from CT scans, there is some variability between subjects due to differences in bone geometry. This inherently created some variation when defining soft tissue attachment sites in a local reference frame.

There are many future steps for this computational model. Firstly, most of the limitations just discussed can be overcome without too much difficulty. MRI data can be taken for geometrical, inertial, and soft-tissue parameters and input into the model. Muscle and ligament wrap around can be incorporated based off of previously described algorithms (Hefzy and Grood, 1983; Blankevoort et al., 1991). Actual real-time flexion temporal functions can be used, although extreme caution should be taken if the motions

are not standardized. Furthermore, the registration software can be programmed to actually output kinematics based upon whatever coordinate system is desired, such as the popular Grood and Suntay system (1983), the Pennock and Clark system (1990), or the more recent system proposed by McPherson et al. (2005). The registration software has already been modified with the capability to manually choose and/or enter soft-tissue attachment sites, which will help to eliminate some of the error associated with using population-based parameters. However, at the time of this writing, this technique had not been utilized in the computational lower limb model. In addition to overcoming the discussed limitations, this model will be applied to more studies, such as comparing the kinetics associated with different TKA implant designs. Eventually, the model will be incorporated into TKA implant design. Design parameters will be optimized by evaluating the predicted *in vivo* kinetics associated with a particular design idea. Designs will be guided based off of principles such as the minimization of tibiofemoral contact forces, ligament strains, or quadriceps loads. This 3-D *in vivo* computational model will be aimed at helping to significantly improve TKA design methodology and processes, thus improving the quality of life in TKA patients themselves.

References

1. Abdel-Rahman E.M., Hefzy M.S., 1998. Three-dimensional behaviour of the human knee joint under impact loading. *Medical Engineering & Physics* 20: 276-290.

2. Alford KS, Komistek RD, Mahfouz MR, Dennis DA, 2005. In vivo correlation of wear, hip separation, and 3-D dynamics of subjects with total hip arthroplasty. In Proceedings of the 72nd American Academy of Orthopaedic Surgeons, Washington D.C.

3. Amis A.A., Bull A.M.J., Gupte C.M., Hijazi I., Race A., Robinson J.R., 2003. Biomechanics of the PCL and related structures: posterolateral, posteromedial and meniscofemoral ligaments. *Knee Surgery, Sports Traumatology, Arthroscopy* 11:271-281.

4. Andriacchi T.P., Yoder D., Conley A., Rosenberg A., Sum J., Galante J.O., 1997. Patellofemoral design influences function following total knee arthroplasty. *Journal of Arthroplasty* 12: 243-249

5. Andriacchi T.P., Alexander E.J., Toney M.K., Dyrby C.O., Sum J., 1998. A point cluster method for in vivo motion analysis: Applied to a study of knee kinematics. *Journal of Biomechanical Eng*ineering 120(6): 743-749.

6. Arnockzky S.P., 1983. Anatomy of the anterior cruciate ligament. *Clinical Orthopaedics* 172: 19-25.

7. Bergmann G., Graichen F., Rohlmann A., 1993. Hip joint loading during walking and running, measured in two patients. *Journal of Biomechanics* 26(8): 969-990.

8. Bergmann G., Deuretzbacher G., Heller M., Graichen F., Rohlmann A., Strauss J., Duda G.N., 2001. Hip contact forces and gait patterns from routine activities. *Journal of Biomechanics* 34: 859-871.

9. Blankevoort L., Kuiper J.H., Huiskes R., Grootenboer H.J., 1991. Articulating contact in a three-dimensional model of the knee. *Journal of Biomechanics* 24(11): 1019-1031.

10. Bristol R.E., Fitzpatrick D.C., Brown T.D., Callaghan, 1996. Non-uniformity of contact stress on polyethylene inserts in total knee arthroplasty. *Clinical Biomechanics* 11(2): 75-80.

11. Burks R.T., 1990. Gross anatomy. In: Daniel D.M., Akeson W.H., O'Connor J.J. (Eds.), Knee Ligaments: Structure, Function, Injury, and Repair. Raven Press, New York. pp. 59-76.

12. Caruntu D.I., Hefzy M.S., 2004. 3-D anatomically based dynamic modeling of the human knee to include tibio-femoral and patello-femoral joints. *Journal of Biomechanical Engineering* 126: 44-53.

13. Challis J.H., 1997. Producing physiologically realistic individual muscle force estimations by imposing constraints when using optimization techniques. *Medical Engineering & Physics* 19(3):253-261.

14. Churchill D.L., Incavo S.J., Johnson C.C., Beynnon B.D., The influence of femoral rollback on patellofemoral contact loads in total knee arthroplasty. *Journal of Arthroplasty* 16(7): 909-918.

15. Clément B., Drouin G., Shorrock G., Gely P., 1989. Statistical analysis of knee ligament lengths. *Journal of Biomechanics* 22(8/9): 767-774.

16. Coughlin K.M., Incavo S.J., Churchill D.L., Beynnon B.D., 2003. Tibial axis and patellar position relative to the femoral epicondylar axis during squatting. *Journal of Arthroplasty* 18(8): 1048-1055.

17. Crowninshield R.D., Johnston R.C., Andrews J.G., Brand R.A., 1978. A biomechanical investigation of the human hip. *Journal of Biomechanics* 11:75-85.

18. Crowninshield R.D., Brand R.A., 1981. A physiologically based criterion of muscle force prediction in locomotion. *Journal of Biomechanics* 14:793-801, 1981.

19. Dennis D.A., Komistek R.A., Hoff W.A., Gabriel S.M., 1996. In vivo kinematics derived using an inverse perspective technique. *Clinical Orthopaedics* 331:107-117.

20. Dennis D.A., Komistek R.D., Colwell C.E., Ranawat C.S., Scott R.D., Thornhill T.S., Lapp M.A., 1998. In vivo anteroposterior femorotibial translation of total knee arthroplasty: a multicenter analysis. *Clinical Orthopaedics* 356:47-57.

21. D'Lima D.D., Hermida J.C., Chen P.C., Colwell C.W., 2001a. Polyethylene wear and variations in knee kinematics. *Clinical Orthopaedics* 392: 124-130.

22. D'Lima D.D., Poole C., Chadha H., Hermida J.C., Mahar A., Colwell C.W., 2001. Quadriceps moments arm and quadriceps forces after total knee arthroplasty. *Clinical Orthopaedics* 392: 213-220.

23. D'Lima D.D., Chen P.C., Colwell C.W., 2001c. Polyethylene contact stresses, articular congruity, and knee alignment. *Clinical Orthopaedics* 392: 232-238.

24. D'Lima D.D., Chen P.C., Kester M.A., Colwell C.W., 2003. Impact of patellofemoral design on patellofemoral forces and polyethylene stresses. *Journal of Bone and Joint Surgery* 85A Suppl. 4: 85-93.

25. Essinger J.R., Leyvraz P.F., Heegard J.H., Robertson D.D., 1989. A mathematical model for the evaluation of the behaviour during flexion of condylar-type knee prostheses. *Journal of Biomechanics* 22(11/12): 1229-1241.

26. Fantozzi S., Leardini A., Banks S.A., Marcacci M., Gianni S., Catani F., 2004. Dynamic in-vivo tibio-femoral and bearing motions in mobile bearing knee arthroplasty. *Knee Surgery, Sports Traumatology, Arthroscopy* 12(2): 144-151.

27. Fleming B.C., Brattbakk B., Peura G.D., Badger G.J., Beynnon B.D., 2002. Measurement of anterior-posterior knee laxity: a comparison of three techniques. *Journal of Orthopaedic Research.* 20:421-426.

28. Ganjika S., Duval N., Yahia L., Guise J., 2000. Three-dimensional knee analyzer validation by simple fluoroscopic study. *Knee* 7: 221-231.

29. Gill H.S., O'Connor J.J., 1996. Biarticulating two-dimensional computer model of the human patellofemoral joint. *Clinical Biomechanics* 11(2): 81-89.

30. Grood E.S., Hefzy M.S., 1982. An analytical technique for modeling knee joint stiffness-part I: ligamentous forces. *Journal of Biomechanical Engineering* 104: 330-337.

31. Grood E.S., Suntay W.J., 1983. A joint coordinate system for the clinical description of three-dimensional motions: application to the knee. *Journal of Biomechanical Engineering* 105: 136-144.

32. Halloran J.P., Petrella A.J., Rullkoetter P.J., 2005. Explicit finite element modeling of total knee replacement mechanics. *Journal of Biomechanics* 38: 323-331.

33. Hanavan E.P., 1964. A mathematical model of the human body. M.S. thesis, Aerospace Medical Research Laboratories, Wright-Patterson Air Force Base, Ohio.

34. Harfe D.T., Chuinard C.R., Espinoza L.M., Thomas K.A., 1998. Elongation patterns of the collateral ligaments of the human knee. *Clinical Biomechanics* 13(3): 163-175.

35. Hefzy M.S., Grood E.S., 1983. An analytical technique for modeling knee joint stiffness-Part II: Ligamentous geometric nonlinearities. *Journal of Biomechanical Engineering* 105: 145-153.

36. Hinrichs R.N., 1990. Adjustments to the segment center of mass proportions of Clauser *et al.* (1969). *Journal of Biomechanics* 23(9): 949-951.

37. Hoff W.A., Komistek R.D., Dennis D.A., Gabriel S.A., Walker S.A., 1998. A three dimensional determination of femorotibial contact positions under in vivo conditions using fluoroscopy. *Journal of Clinical Biomechanics* 13: 455-470.

38. Hsu H.-P., Walker P.S., Wear and deformation of patellar components in total knee arthroplasty. *Clinical Orthopaedics* 246: 260-265.

39. Hungerford D.S., Barry M., 1979. Biomechanics of the patellofemoral joint. *Clinical Orthopaedics* 144: 9-15.

40. Hughston J.C., Bowden J.A., Andrews J.R., Norwood L.A., 1980. Acute tears of the posterior cruciate ligament. *Journal of Bone and Joint Surgery* 62A: 438-450.

41. Kane T.R., Levinson D.A., 2000. Dynamics Online: Theory and Implementation with AUTOLEV^{TM}, Online Dynamics Inc., Sunnyvale, CA.

42. Kane T.R., Levinson D.A., 1985. Dynamics: Theory and Applications. McGraw-Hill, New York.

43. Kanisawa I., Banks A.Z., Banks S.A., Moriya H., Tsuchiya A., 2003. Weight-bearing kinematics in subjects with two types of anterior cruciate ligament reconstructions. *Knee Surgery, Sports Traumatology, Arthroscopy* 11:16-22.

44. Kennedy J.C., Hawkins R.J., Willis R.B., Danylcuck K.D., 1976. Tension studies of human knee ligaments. Yield point, ultimate failure, and disruption of the cruciate and tibial collateral ligaments. *Journal of Bone and Joint Surgery* 58A: 350-355.

45. Komistek R.D., Stiehl J.B., Dennis D.A., Paxson R.D., Soutas-Little R.W., 1998. Mathematical model of the lower extremity joint reaction forces using Kane's method of dynamics. *Journal of Biomechanics* 31:185-189.

46. Komistek R.D., Dennis D.A., Mahfouz M.R., 2003. In vivo fluoroscopic analysis of the normal knee. *Clinical Orthopaedics* 410: 69-81.

47. LaFortune M.A., Cavanagh P.R., Sommer III H.J., Kalenak A., 1992. Three-dimensional kinematics of the human knee during walking. *Journal of Biomechanics* 25(4): 347-357.

48. Liau J.J., Cheng C.K., Huang C.H., Lo W.H., 2002. The effect of malalignment on stresses in polyethylene component of total knee prostheses – a finite element analysis. *Clinical Biomechanics* 17: 140-146.

49. Lin F., Makhsous M., Chang A.H., Hendrix R.W., Zhang L.Q., 2003. In vivo and noninvasive six degrees of freedom patellar tracking during voluntary knee movement. *Clinical Biomechanics* 18: 401-409.

50. Li G., Kaufman K.R., Chao E.Y.S., Rubash H.E., 1999a. Prediction of antagonistic muscle forces using an inverse dynamic optimization during flexion/extension of the knee. *Journal of Biomechanical Engineering* 121:316-322.

51. Li G., Gil J., Kanamori A., Woo S.L.-Y., 1999b. A validated three-dimensional computational model of a human knee joint. *Journal of Biomechanical Engineering* 121: 657-662.

52. Li G., Zayontz S., Most E., Otterberg E., Sabbag K., Rubash H.E., 2001. Cruciate-retaining and cruciate-substituting total knee arthroplasty. *Journal of Arthroplasty* 16(8 Suppl. 1): 150-156.

53. Li G., DeFrate L.E., Sun H., Gill T.J., 2004. In vivo elongation of the anterior cruciate ligament and posterior cruciate ligament during knee flexion. *American Journal of Sports Medicine* 32(6): 1415-1420.

54. Lloyd D.G., Besier T.F., 2003. An EMG-driven musculoskeletal model to estimate muscle forces and knee joint moments in vivo. *Journal of Biomechanics* 36: 765-776.

55. Mahfouz M.R., Hoff W.A., Komistek R.D., Dennis D.A., 2003. A robust method for registration of three-dimensional knee implant models to two-dimensional fluoroscopy images. *IEEE Transactions on Medical Imaging* 22(12): 1561-1574.

56. Mahoney O.M., Noble P.C., Rhoads D.D., Alexander J.W., Tullos H.S., 1994. Posterior cruciate function following total knee arthroplasty. A biomechanical study. *Journal of Arthroplasty* 9(6): 569-578.

57. Marin F., Allain J., Diop A., Maurel N., Simondi M., Lavaste F., 1999. On the estimation of knee joint kinematics. *Human Movement Science* 18: 613-626.

58. McPherson A., Karrholm J, Pinskerova V., Sosna A., Martelli S., 2005. Imaging knee position using MRI, RSA/CT and 3D digitisation. *Journal of Biomechanics* 38(2): 263-268.

59. Miura H., Higaki H., Nakanishi Y., Mawatari T., Moro-oka T., Murakami T., Iwamoto Y., 2002. Prediction of total knee arthroplasty polyethylene wear using the wear index. *Journal of Arthroplasty* 17(6): 760-766.

60. Mommersteeg T.J.A., Huiskes R., Blankevoort L., Kooloos J.G.M., Kauer J.M.G., 1997. An inverse dynamics approach to determine the restraining function of human knee ligament bundles. *Journal of Biomechanics* 30(2): 139-146.

61. Most E., Zayontz S., Li G., Otterberg E., Sabbag K., Rubash H.E., 2003. Femoral rollback after cruciate-retaining and stabilizing total knee arthroplasty. *Clinical Orthopaedics* 410: 101-113.

62. Murphy M.C., 1990. Geometry and the kinematics of the normal human knee. PhD Thesis, MIT.

63. Norwood L.A., Cross M.J., Anterior cruciate ligament: functional anatomy of its bundles in rotary instabilities. *American Journal of Sports Medicine* 7(1): 23-26.

64. Nozaki H., Banks S.A., Suguro T., Hodege W.A., 2002. Observations of femoral rollback in cruciate-retaining knee arthroplasty. *Clinical Orthopaedics* 404: 308-314.

65. Otter A.R., Geurts A.C.H., Mulder T., Duysens J., 2004. Speed related changes in muscle activity from normal to very slow walking speeds. *Gait and Posture* 19: 270-278.

66. Paul, J.P., 1965. Bio-engineering studies of the forces transmitted by joints. engineering analysis, In Biomechanics and Related Bio-Engineering Topics, 369-380. Edited by R. M. Kenedi, Pergamon Press, Oxford.

67. Pennock G.R., Clark K.J., 1990. An anatomy-based coordinate system for the description of the kinematic displacements in the human knee. *Journal of Biomechanics* 23(12): 1209-1218.

68. Pierrynowski M.R., Morrison J.B., 1985. Estimating the muscle forces generated in the human lower extremity when walking: a physiological solution. *Mathematical Biosciences* 75:43-68.

69. Ramsey D.K., Wretenberg P.F., Benoit D.L., Lamontagne M., Németh G., 2003. Methodological concerns using intra-cortical pins to measure tibiofemoral kinematics. *Knee Surgery, Sports Traumatology, Arthroscopy* 11(5): 344-349.

70. Reinschmidt C., van den Bogart A.J., Nigg B.M., Lundberg A., Murphy N., 1997. Effect of skin movement on the analysis of skeletal knee joint motion during running. *Journal of Biomechanics* 30(7): 729-732.

71. Rydell N., 1965. Intravital measurements of forces acting on the hip-joint. In Evans FG (Ed.), Studies on the Anatomy and Function of Bone and Joints. Springer-Verlag, Berlin, pp. 52-68.

72. Saari T., Uvehammer J., Carlsson L.V., Herberts P., Regner L., Karrholm J., 2003. Kinematics of three variations of the Freeman-Samuelson total knee prosthesis. *Clinical Orthopaedics* 410: 235-247.

73. Seireg A., Avrikar R.J., 1975. The prediction of muscular load sharing and joint forces in the lower extremities during walking. *Journal of Biomechanics* 8: 89-102.

74. Shelburne K.B., Pandy M.G., 1997. A musculoskeletal model of the knee for evaluating ligament forces during isometric contractions. *Journal of Biomechanics* 30(2): 163-176.

75. Singerman R., Berilla J., Archdeacon M., Peyser A., 1999. In vitro forces in the normal and cruciate-deficient knee during simulated squatting motion. *Journal of Biomechanical Engineering* 121: 234-242.

76. Soutas-Little R.W., Beavis G.C., Verstraete M.C., Markus T.L., 1987. Analysis of foot motion during running using a joint co-ordinate system. *Medicine and Science in Sports and Exercise* 19(3): 285-293.

77. Tamhane A.C., Dunlop D.D., 2000. Statistics and Data Analysis: from Elementary to Intermediate. Prentice-Hall, Upper Saddle River, NJ, pp. 279-282.

78. Taylor M., Barrett D.S., 2003. Explicit finite element simulation of eccentric loading in total knee replacement. *Clinical Orthopaedics* 414:162-171.

79. Taylor S.J.G., Perry J.S., Meswania J.M., Donaldson N., Walker P.S., Cannon S.R., 1997. Telemetry of forces from proximal femoral replacements and relevance to fixation. *Journal of Biomechanics* 30(3): 225-234.

80. Taylor S.J.G., Walker P.S., 2001. Forces and moments telemetered from two distal femoral replacements during various activities. *Journal of Biomechanics* 34:839-848.

81. Toutoungi D.E., Lu T.W., Leardini A., Catani F., O'Connor J.J., 2000. Cruciate ligament forces in the human knee during rehabilitation exercises. *Clinical Biomechanics* 15:176-187.

82. Trent P.S., Walker P.S., Wolf B., 1976. Ligament length patterns, strength, and rotational axes of the knee joint. *Clinical Orthopaedics* 117:263-270.

83. Walker P.S., Blunn G.W., Broome D.R., Perry J., Watkins A., Sathasivam S., Dewar M.E., Paul J.P., 1997. A knee simulating machine for performance evaluation of total knee replacements. *Journal of Biomechanics* 30(1): 83-89.

84. Wang C.-J., Walker P.S., 1973. The effects of flexion and rotation on the length patterns of the ligaments of the knee. *Journal of Biomechanics* 6: 587-596.

85. White S.C., Yack H.J., Winter D.A., 1989. A three-dimensional musculoskeletal model for gait analysis: anatomical variability estimates. *Journal of Biomechanics* 22(8/9): 885-893.

86. Yoshiya S., Komistek R.D., Matsui N., Maruyama S., Kurosaka M., 2004. In vivo kinematic analysis of deep knee flexion after total knee arthroplasty. In Proceedings of the 71st American Academy of Orthopaedic Surgeons, San Francisco.

Appendices

Appendix A: Geometrical Parameters

Table A.1: Raw data for geometrical parameters.

Femoral data points				
Origin of fem coord system at greater trochanter				
	X (cm)	**Y (cm)**	**Z (cm)**	
greater trochanter (most lateral projection)	0	0	0	
femoral head (center)	0	3	-8.2	
medial epicondyle tip	-3.1	-40.3	-12.5	
lateral epicondyle tip	-2	-40.9	-2.8	
knee joint center	-2.3	-43.5	-8.2	
Vastus intermedius	1.7	-14.7	-4	
Resulting femoral length (distance from femoral head to knee joint center):			**0.46556847 m**	
Tibial data points				
Origin of tib coord system at tibial tuberosity				
tibial tuberosity	0	0	0	
knee joint center	-3.5	4.8	-0.4	
ankle joint center	-5.2	-33.8	-2.7	
medial malleolus	-4.8	-32.2	-5.2	
lateral malleolus	-6	-34.3	0.1	
malleoli mid point	-5.4	-33.25	-2.55	
Resulting tibial length (distance from knee joint center to mid-malleoli point):			**0.38158027 m**	

Table A.2: Data for geometrical parameters converted to fit the coordinate system utilized in the model. Data corresponds to a left leg facing left.

Femoral data points							
Origin of fem coord system at knee joint center; left leg facing left; +x=posterior, +y=superior, +z=lateral				Origin of fem coord system at fem-component-centroid; left leg facing left; +x=posterior, +y=superior, +z=lateral			
	X (m)	**Y (m)**	**Z (m)**		**X (m)**	**Y (m)**	**Z (m)**
greater trochanter (most lateral projection)	-0.023	0.435	0.082	greater trochanter (most lateral projection)	-0.023	0.405	0.082
femoral head (center)	-0.023	0.465	0.000	femoral head (center)	-0.023	0.435	0.000
medial epicondyle tip	0.008	0.032	-0.043	medial epicondyle tip	0.008	0.002	-0.043
lateral epicondyle tip	-0.003	0.026	0.054	lateral epicondyle tip	-0.003	-0.004	0.054
knee joint center	0.000	0.000	0.000	knee joint center	0.000	-0.030	0.000
Vastus intermedius	-0.04	0.288	0.042	Vastus intermedius	-0.040	0.258	0.042
Tibial data points							
Origin of tib coord system at knee joint center				Origin of fem coord system at tib-component-centroid			
tibial tuberosity	-0.035	-0.048	0.004	tibial tuberosity	-0.035	-0.018	0.004
knee joint center	0	0	0	knee joint center	0	0.03	0
ankle joint center	0.017	-0.386	-0.023	ankle joint center	0.017	-0.356	-0.023
medial malleolus	0.013	-0.37	-0.048	medial malleolus	0.013	-0.34	-0.048
lateral malleolus	0.025	-0.391	0.005	lateral malleolus	0.025	-0.361	0.005
malleoli mid point	0.019	-0.3805	-0.0215	malleoli mid point	0.019	-0.3505	-0.0215

Table A.3: Segment masses utilized within the model.

	Mass (proportion of body mass)	Applied to model (kg)
thigh	0.11	8.4832
shank	0.047	3.62464

Table A.4: Locations of the centers of mass used within the model.

	proportion of length	distance (m)
knee joint center to femoral CM	0.4001	0.186
knee joint center to tibial CM	0.4179	0.159

Appendix B: Inertial Parameters and Theory

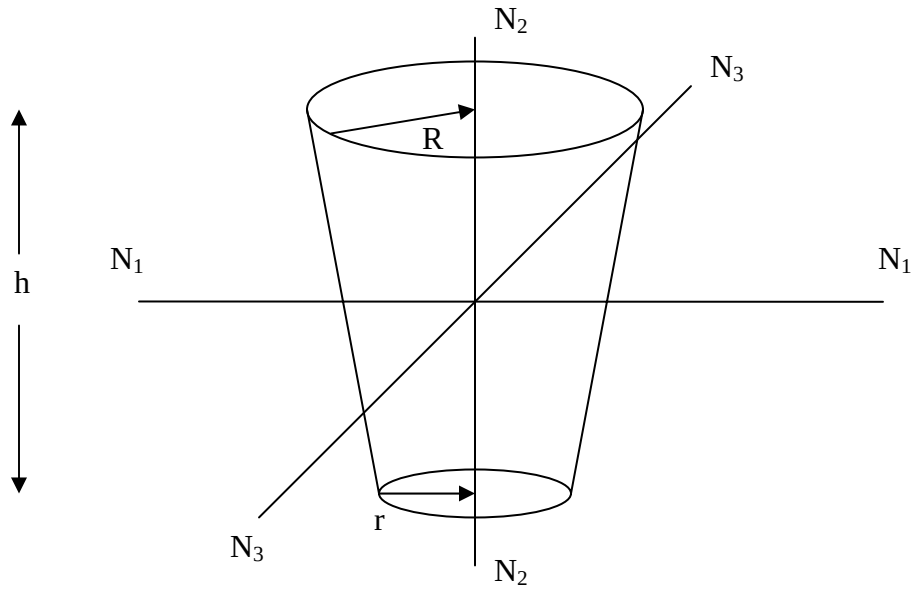

Figure B.1: Frustum of right circular cone model for limb segments.

Figure B.1 contains the right circular cone frustum model utilized to calculate the inertial properties of the lower limb segments, the thigh and shank, within the computational model. All theory is from Hanavan's study on creating a model of the human body (1964). Start by defining μ and σ:

$$\mu = \frac{r}{R}, \tag{B.1}$$

and

$$\sigma = 1 + \mu + \mu^2 . \tag{B.2}$$

The density of the frustum is given by

$$\rho = \frac{3M}{\pi R^2 h \sigma}, \tag{B.3}$$

where M is the segment mass, given in Table B.3. Then the moments of inertia of the frustum, I_{11}, I_{22}, and I_{33}, about the three orthogonal axes, N_1, N_2, and N_3 through the center of mass are given by:

$$I_{11} = M\left[\left(\frac{9}{20\pi} * \frac{1+\mu+\mu^2+\mu^3+\mu^4}{\sigma^2} * \frac{M}{\rho h}\right) + \left(\frac{3}{80} * \frac{1+4\mu+10\mu^2+4\mu^3+\mu^4}{\sigma^2} * h^2\right)\right], \tag{B.4}$$

$$I_{22} = \frac{2M^2}{\rho h}\frac{9}{20\pi}\frac{1+\mu+\mu^2+\mu^3+\mu^4}{\sigma^2}, \tag{B.5}$$

and

$$I_{33} = M\left[\left(\frac{9}{20\pi} * \frac{1+\mu+\mu^2+\mu^3+\mu^4}{\sigma^2} * \frac{M}{\rho h}\right) + \left(\frac{3}{80} * \frac{1+4\mu+10\mu^2+4\mu^3+\mu^4}{\sigma^2} * h^2\right)\right]. \tag{B.6}$$

The measurements taken from a sample male, 1.88 m tall and of mass 77.1 kg, are given in Table B.1.

Table B.1: Measurements taken from a sample human (mass = 77.1 kg, height = 1.88 m).

Dimension/Segment	Circumference (in)	Circumference (m)	radius (m)
upper thigh	24	0.6096	0.09702085
lower thigh	16	0.4064	0.06468057
upper shank	14	0.3556	0.0565955
lower shank	10.5	0.2667	0.04244662
length thigh	16.5	0.4191	n/a
length shank	18	0.4572	n/a

Appendix C: Ligament Parameters

Table C.1: Raw Data for ligament attachment sites (from Abdel-Rahman et al., 1998).

Ligament	Femoral attachments Origin of fem coord system at knee joint center			Tibial attachments Origin at tibial Center of Mass		
	X (cm)	Y (cm)	Z (cm)	X(cm)	Y(cm)	Z(cm)
MCL (anterior fibers)	-3.475	-0.1	2.625	-2	0.4	17.125
MCL (oblique)	-3.475	-0.8	2.425	-3.5	-3	19.925
MCL (deep)	-3.475	-0.5	2.125	-3.5	0	19.925
LCL	3.525	-1.5	2.125	4.5	-2.5	17.625
ACL (ant-med)	0.725	-1.56	2.125	-0.7	0.5	21.125
ACL (post-lat)	0.725	-2.03	1.955	0.2	0.2	21.225
PCL (ant-lat)	-0.475	-1.12	1.405	0.5	-3	20.625
PCL (post-med)	-0.475	-2.32	1.565	-0.5	-3	20.625

Table C.2: Ligament attachment site data transformed to fit the model coordinate systems. Assumed tibial model centroid was 5 cm distal to the knee joint center; femoral model centroid was 4 cm proximal to the knee joint center.

Ligament	Femoral Attachments Origin at femoral model center			Tibial Attachments Origin at tibial model center		
	X(m)	Y (m)	Z(m)	X(m)	Y (m)	Z(m)
MCL (anterior fibers)	0.001	-0.01375	0.03475	-0.004	-0.00375	0.02
MCL (oblique)	0.008	-0.01575	0.03475	0.03	0.02425	0.035
MCL (deep)	0.005	-0.01875	0.03475	0	0.02425	0.035
LCL	0.015	-0.01875	-0.03525	0.025	0.00125	-0.045
ACL (ant-med)	0.0156	-0.01875	-0.00725	-0.005	0.03625	0.007
ACL (post-lat)	0.0203	-0.02045	-0.00725	-0.002	0.03725	-0.002
PCL (ant-lat)	0.0112	-0.02595	0.00475	0.03	0.03125	-0.005
PCL (post-med)	0.0232	-0.02435	0.00475	0.03	0.03125	0.005

Table C.3: Ligament extension ratios (at full extension; Abdel-Rahman and Hefzy, 1998) and stiffness coefficients, k (Li et al., 1999b).

Ligament	extension ratio	k (N)
MCL (anterior	0.94	2750
MCL (oblique)	1.031	2750
MCL (deep)	1.049	1000
LCL	1.05	2000
ACL (ant-med)	1	5000
ACL (post-lat)	1.051	5000
PCL (ant-lat)	1.004	9000
PCL (post-med)	1.05	9000

Vita

Joel Thomas Outten was born in Cookeville, TN, on February 18th, 1980. He moved to Greenville, South Carolina in 2nd grade, then off to Cincinnati, OH in 9th grade. After graduating, he enrolled at the University of Tennessee in Engineering Science (the pre-Biomedical Engineering program). After a year or so, he decided to minor in Mathematics as well, then, maybe a year later, decided to go ahead and go for the double major instead. Eventually, he got involved with some finite-element vascular work at the UT Medical Center and Oak Ridge National Laboratory. He graduated in December, 2003 with a B.S. in Engineering Science, and the Math secondary major, and kept on with the vascular modeling for a bit. After attending bartending-school and finishing up the vascular modeling, he hesitantly made the switch to biomechanics and orthopaedics. He began in M.S. in Fall, 2004, and found that orthopaedics grew on him quite a bit. He graduated with a M.S. in Engineering Science, with a minor in Statistics, in Spring, 2005.

Whatever he's doing now, he's probably spending his spare time hiking, camping, playing guitar, cursing himself for not playing more tennis, and maybe making use of that bartending degree.